REPORT DOCUMENTATION PAGE

Form Approved OMB NO. 0704-0188

1. REPORT DATE (DD-MM-YYYY)	2. REPORT TYPE	3. DATES COVERED (From - To)
31-08-2021	Final Report	15-Sep-2017 - 14-Mar-2021

4. TITLE AND SUBTITLE
Final Report: Magnetoelectronic Sensors for Gasotransmitters

5a. CONTRACT NUMBER
W911NF-17-1-0398

5b. GRANT NUMBER

5c. PROGRAM ELEMENT NUMBER
611102

6. AUTHORS

5d. PROJECT NUMBER

5e. TASK NUMBER

5f. WORK UNIT NUMBER

7. PERFORMING ORGANIZATION NAMES AND ADDRESSES
Dartmouth College
11 Rope Ferry Rd.

Hanover, NH 03755 -1404

8. PERFORMING ORGANIZATION REPORT NUMBER

9. SPONSORING/MONITORING AGENCY NAME(S) AND ADDRESS (ES)
U.S. Army Research Office
P.O. Box 12211
Research Triangle Park, NC 27709-2211

10. SPONSOR/MONITOR'S ACRONYM(S)
ARO

11. SPONSOR/MONITOR'S REPORT NUMBER(S)
70871-MS-YIP.24

12. DISTRIBUTION AVAILIBILITY STATEMENT
Approved for public release; distribution is unlimited.

13. SUPPLEMENTARY NOTES
The views, opinions and/or findings contained in this report are those of the author(s) and should not contrued as an official Department of the Army position, policy or decision, unless so designated by other documentation.

14. ABSTRACT

15. SUBJECT TERMS

16. SECURITY CLASSIFICATION OF:			17. LIMITATION OF ABSTRACT	15. NUMBER OF PAGES	19a. NAME OF RESPONSIBLE PERSON
a. REPORT	b. ABSTRACT	c. THIS PAGE			Katherine Mirica
UU	UU	UU	UU		19b. TELEPHONE NUMBER 603-646-8188

RPPR Final Report
as of 31-Aug-2021

Agency Code: 21XD

Proposal Number: 70871MSYIP **Agreement Number: W911NF-17-1-0398**
INVESTIGATOR(S):

Name: Katherine Mirica
Email: katherine.a.mirica@dartmouth.edu
Phone Number: 6036468188
Principal: Y

Organization: **Dartmouth College**
Address: 11 Rope Ferry Rd., Hanover, NH 037551404
Country: USA
DUNS Number: 041027822 EIN: 020222111

Report Date: 14-Jun-2021 Date Received: 31-Aug-2021
Final Report for Period Beginning 15-Sep-2017 and Ending 14-Mar-2021
Title: Magnetoelectronic Sensors for Gasotransmitters
Begin Performance Period: 15-Sep-2017 **End Performance Period:** 14-Mar-2021
Report Term: 0-Other

Submitted By: Katherine Mirica Email: katherine.a.mirica@dartmouth.edu
Phone: (603) 646-8188

STEM Degrees: 2 **STEM Participants:**

Major Goals: This proposal focuses on addressing the analytical challenge of detecting gasotransmitters. The experimental approach relies on developing new materials and a new paradigm in signal transduction and amplification in solid-state chemical sensors that takes advantage of two fundamental properties of electrons: charge and spin. The molecular design towards this goal employs bottom-up synthesis of multifunctional responsive two-dimensional (2D) nanomaterials capable of changing their electrical resistance in response to a chemical stimulus due to perturbations of both electronic and magnetic properties.

The research in the proposal is organized into three major goals. Each major goal is subdivided into a set of sub-goals, which are then executed using a discrete set of tasks.

Major Goal 1: Molecular design and synthesis of magnetoelectronic materials having stimuli-responsive magnetic and electronic properties.

1.1. Molecular Design of Receptors

1.1.1. Computational assessment of analyte-MOF interactions using molecular analog of metal bis(dioxolene) receptors. Milestone: Computed minimized structures, binding affinities, and spin densities for molecular MOF analogs interacting with analytes. Progress: 100 % complete (Fig. 1-2).

1.1.2. Computational assessment of analyte-COF interactions using molecular analog of metal phthalocyanine (MPc) receptors. Milestone: Computed minimized structures, binding affinities, and spin densities for MPc units interacting with analytes. Progress: 100 % complete (Fig. 3).

1.2. Molecular Design of Stimuli-Responsive Materials

1.2.1. Computational examination of the influence of metal and ligand on band gap of MOF monolayers. Milestone: Computed minimized structures, band structures, and band gaps for MOF monolayers. Progress: 100 % complete (Fig. 4).

1.2.2. Computational assessment of the influence of MPc subunit and covalent linkers on the band gap of COFs monolayers. Milestone: Computed minimized structures, band structures, and band gaps for COF monolayers. Progress: 100 % complete. (Fig. 5-6).

1.3. Design and Synthesis of Stimuli-Responsive MOFs

1.3.1. Optimization of morphological control for producing free-standing MOF nanowires and nanosheets. Milestone: Publication quality and statistically significant SEM images and X-Ray diffractograms characterizing MOF nanowires and nanosheets. Progress: 100 % complete (Fig. 7-8).

1.3.2. Computational assessment of the influence of metal and ligand on the anisotropy of charge transport in MOF nanorods. Milestone: Modeled crystalline substructures of different MOF analogs in Material Studio to compute electron transport through-stack and through-sheet. Progress: 100 %. (Fig. 9)

1.3.3. Computational assessment of the influence of metal and ligand on the anisotropy of charge transport in MOF nanosheets. Milestone: Modeled crystalline substructures of different MOF analogs in Material Studio to compute electron transport through-stack and through-sheet. Progress: 100 %. (Fig. 9)

1.4. Design and Synthesis of Stimuli-Responsive COFs

1.4.1. Synthesis and characterization of MPc-based molecular precursors to COFs. Milestone: Optimized synthetic access and rigorous characterization using the combination of NMR, IR, Mass Spectrometry, and Elemental Analysis. Progress: 100 % complete (Fig. 10-12).

1.4.2. Synthesis and characterization of MPc-based COFs. Milestone: Optimized synthetic access and rigorous materials characterization using pXRD, BET, SEM, and TEM. Progress: 100 % complete (Fig. 13-14).

1.4.3. Optimization of morphological control within MPc-based COFs. Publication quality and statistically significant SEM images and X-Ray diffractograms characterizing COF morphology as a function of synthetic conditions. Progress: 100 % complete (Fig. 15).

Major Goal 2: Studies of structure-property relationships in these materials in solid-state devices.

2.1. Studies of Electrical Properties of MOFs and COFs

2.1.1. Measurement of conductivity of MOFs having highly tuned morphological control. Milestone: Measured conductivity of MOF nanowires and nanosheets. Progress: 100% Complete (Fig. 16).

2.1.2. Examination of the impact of the electrodes on device performance in MOFs. Milestone: Measurements of the influence of the electrode type upon sensing performance of MOF in response to target analytes. Progress: 100% complete (Fig. 17).

2.1.3. Measurement of conductivity of COFs having tuned morphological control. Measured conductivity of COF nanocrystals. Progress: 100 % complete (Fig. 18).

2.1.4. Examination of the impact of the electrodes on device performance in COFs. The progress on this task was disrupted due to COVID-19 pandemic.

2.2. Studies of Magnetic Properties of MOFs and COFs

2.2.1. EPR studies of analyte binding in MOFs. Milestone: Measured perturbations to the concentration and chemical environment of unpaired spins in conductive MOFs as they bind gaseous analytes using electron paramagnetic spectroscopy and X-ray photoelectron spectroscopy. Progress: 100 % complete (Fig. 19-23).

2.2.2. EPR studies of analyte binding in COFs. Measured perturbations to the concentration and chemical environment of unpaired spins in conductive COFs as they bind gaseous analytes electron paramagnetic spectroscopy. Progress: 100 % complete (Fig. 24-25).

2.2.3. SQUID magnetometry of MOFs. Milestone: Characterize magnetic ordering in MOFs. Progress: 100 % complete (Fig. 26).

2.2.4. SQUID magnetometry of COFs. Milestone: Characterize magnetic ordering in COFs. Due to COVID-19 pandemic, magnetic properties were assessed computationally Progress: 100 % complete (Fig. 27).

Major Goal 3: Magnetoelectronic signal amplification and selective detection of CO, NO, and H2S using solid state devices.

3.1. Studies of Coupled Conductivity and Magnetism in MOFs and COFs.

3.1.1. Measurements of microwave conductivity in MOFs. Milestone: Measured microwave conductivity in MOFs in the presence and absence of analytes. Due to travel restrictions, necessary instrumentation was not accessible to complete this task as anticipated. (Table 1)

3.1.2. Measurements of microwave conductivity in COFs. Milestone: Measured microwave conductivity in COFs in the presence and absence of analytes. Due to travel restrictions, necessary instrumentation was not accessible to complete this task as originally anticipated. (Table 2)

3.2. Coupling Chemiresistance with Magnetoresistance

3.2.1. Fabrication of Hall Bar devices with MOFs. Milestone: Reliable fabrication of Hall Bar devices with embedded MOFs. Progress: 20 % complete (Fig. 28-30).

3.2.2. Measurements of charge mobility of MOFs. Milestone: Optimized measurements of charge mobility in MOFs. Progress: 50% complete (Fig. 28, 31).

3.2.3. Measurements of field effect in MOFs. Milestone: Optimized measurements of electric and magnetic field effect in MOFs. Progress: 50% complete (Fig. 28-29).

3.2.4. Measurements of the perturbations of charge mobility and field effect upon CO, NO, and H2S binding to MOFs. Milestone: Optimized measurements of the perturbations to the charge mobility and field effects in MOFs upon analyte exposure. Progress: 100 % complete. (Fig. 32-33)

3.2.5. Fabrication of Hall Bar devices with COFs. Milestone: Reliable fabrication of Hall Bar devices with embedded COFs. This task was disrupted due to COVID-19 restrictions.

3.2.6. Measurements of charge mobility of COFs. Milestone: Optimized measurements of charge mobility in COFs. Progress: 20% complete. (Fig. 34)

3.2.7. Measurements of field effect in COFs. Milestone: Optimized measurements of electric and magnetic field effect in COFs. Progress: 20% complete. (Fig. 34). Progress on this task was disrupted due to COVID-19 restrictions.

3.2.8. Measurements of the perturbations of charge mobility and field effect upon CO, NO, and H2S binding to COFs. Milestone: Optimized measurements of the perturbations of analytes to the charge mobility. Progress: 100% complete. (Fig 35-37).

Accomplishments: please see attached pdf document

RPPR Final Report
as of 31-Aug-2021

Training Opportunities: Training opportunities supported by this grant involved professional development of graduate research assistants in the form of research mentoring and presentations. Specific highlights include:

Trainee Name: Robert M. Stolz
Title of event: Institute seminar, Frontier Institute for Research in Sensor Technologies (FIRST), University of Maine
Role: Presenter
Presentation Title: Host–Guest Interactions and Redox Activity in Layered Conductive Metal–Organic Frameworks
Date: 07/31/2020

Trainee Name: Robert M. Stolz
Title of event: American Chemical Society Spring National Meeting, 2020, San Francisco CA
Role: Presenter
Presentation Title:: Understanding the Surface Chemistry of 2D Conductive MOFs: insight into the role of the interface in electrically-transduced chemical sensing
Date: 08/17/2020–08/20/2020

Trainee Name: Robert M. Stolz
Title of event: Frühjahrssymposium, 2021, Leipzig, Germany
Your role: Presenter and member of the American Delegation
Presentation Title: Mechanisms of Electroanalysis with Conductive Metal–Organic Frameworks
Date: 03/29/2021–04/01/2021

Trainee Name: Robert M. Stolz
Title of event: Northeastern Section Younger Chemists Committee (Northeastern Section of the American Chemical Society), 2021, Boston, MA
Role: Presenter (poster)
Presentation Title: Mechanisms of Electroanalysis with Conductive Metal–Organic Frameworks
Date: 04/24/2021

Trainee Name: Robert M. Stolz
Title of event: JACS in Session with ACS Applied Materials & Interfaces: webinar series, 2021
Role: Attendee
Presentation Title: N/A
Date: 06/08/2021

RPPR Final Report
as of 31-Aug-2021

Results Dissemination: The progress on this project has been disseminated in 13 peer reviewed publications, since the start of this award:

1. Ko, M.; Aykanat, A.; Smith, M. K.; Mirica, K. A.* “Drawing Sensors with Ball-Milled Blends of Metal-Organic Frameworks and Graphite” Sensors 2017, 17, 2192. Invited paper for a special issue “Chemiresistive Sensors: Status and the Future” co-edited with Prof. Timothy M. Swager.

2. Smith, M.; Mirica, K. A.* “Self-Organized Frameworks on Textiles (SOFT): Conductive Fabrics for Simultaneous Sensing, Capture, and Filtration of Gases” J. Am. Chem. Soc. 2017, 139, 16759–16767.

3. Mendecki, L; Mirica, K. A.* “Conductive Metal–Organic Frameworks as Ion-to-Electron Transducers in Potentiometric Sensors" ACS Appl. Mater. Interfaces 2018, 10, 19248–19257.

4. Ko, M.; Mendecki, L.; Mirica, K. A.* "Conductive two-dimensional metal–organic frameworks as multifunctional materials" Chem. Commun. 2018, 54, 7873-7891.

5. Meng, Z.; Stolz, R. M.; Mendecki, L.; Mirica, K. A.* “Electrically-Transduced Chemical Sensors Based on Two-Dimensional Nanomaterials” Chem. Rev. 2019, 119, 478–598.

6. Meng, Z.; Aykanat, A.; Mirica, K. A.* “Proton Conduction in 2D Aza-Fused Covalent Organic Frameworks” Chem. Mater. 2019, 31, 819–825.

7. Meng, Z.; Aykanat, A.; Mirica, K. A.* “Welding Metallophthalocyanines into Bimetallic Molecular Meshes for Ultrasensitive, Low-Power Chemiresistive Detection of Gases” J. Am. Chem. Soc. 2019, 141, 2046–2053.

8. Meng, Z.; Stolz, R.; Mirica, K. A.* “Two-Dimensional Chemiresistive Covalent Organic Framework with High Intrinsic Conductivity” J. Am. Chem. Soc. 2019, 141, 11929–11937.

9. Aykanat, A.; Meng, Z.; Bendetto, G.; Mirica K. A.* “Molecular Engineering of Multifunctional Metallophtalocyanine-Containing Framework Materials” Chem. Mater. 2020, 32, 5372–5409.

10. Ko, M.; Mendecki, L.; Eagleton, A.; Durbin, C. G.; Stolz, R. M.; Meng. Z.; Mirica, K. A.* “Employing Conductive Metal–Organic Frameworks for Voltammetric Detection of Neurochemicals” J. Am. Chem. Soc. 2020, 142, 11717–11733

11. Stolz, R. M.; Mahdavi-Shakib, A.; Frederick, B. G.*; Mirica, K. A.* “Host–Guest Interactions and Redox Activity in Layered Conductive Metal–Organic Frameworks” Chem. Mater. 2020, 32, 7639–7652.

12. Meng, Z.; Luo, J.; Li, W.*; Mirica, K. A.* “Hierarchical Tuning of the Performance of Electrochemical Carbon Dioxide Reduction Using Conductive Two-Dimensional Metallophthalocyanine Based Metal?Organic Frameworks” J. Am. Chem. Soc. 2020, 142, 21656–21669.

13. Meng, Z.; Mirica, K. A.* “Two-Dimensional d-pi Conjugated Metal-Organic Framework Based on Hexahydroxytrinaphthylene” Nano Research 2021, 14, 369–375.

Additionally, the research has been disseminated in 52 research presentations presented by PI.

RPPR Final Report
as of 31-Aug-2021

Honors and Awards: Awards to Katherine Mirica (PI) during 2017-2021:

Karen E. Wetterhahn Memorial Award for Distinguished Creative or Scholarly Achievement (2021)
Gordon Russell 1955 Fellowship, Dartmouth College (2021)
NIH Maximizing Investigators' Research Award (2020)
Camille Dreyfus Teacher Scholar Award (2020)
NSF CAREER Award (2020)
Cottrell Scholar Award (2019)
Alfred P. Sloan Research Fellowship in Chemistry (2018)
3M Non-Tenured Faculty Award (2018)
American Chemical Society PMSE Young Investigator Award (2018)
Thieme Chemistry Journal Award (2018)
Enhanced Junior Faculty Fellowship, Dartmouth College (2018)

Protocol Activity Status:

Technology Transfer: 1. monthly update call with Todd Miller and Natalie Pomerantz at Natick Soldier Center (Natick, MA)
2. collaborative discussions with Caitlyn Callahan at CRREL about other projects (Hanover, NH)
3. collaborative discussions and sample exchange with Gregory Peterson regarding testing metal-organic frameworks on textiles for another project (Aberdeen Proving Ground, MD)

PARTICIPANTS:

Participant Type: PD/PI
Participant: Katherine Mirica
Person Months Worked: 6.00 **Funding Support:**
Project Contribution:
National Academy Member: N

Participant Type: Graduate Student (research assistant)
Participant: Robert Stolz
Person Months Worked: 15.00 **Funding Support:**
Project Contribution:
National Academy Member: N

Participant Type: Graduate Student (research assistant)
Participant: Michael Ko
Person Months Worked: 15.00 **Funding Support:**
Project Contribution:
National Academy Member: N

Participant Type: High School Student
Participant: Katherine MacVeagh
Person Months Worked: 3.00 **Funding Support:**
Project Contribution:
National Academy Member: N

Participant Type: Undergraduate Student
Participant: Adelaide Levenson

RPPR Final Report
as of 31-Aug-2021

Person Months Worked: 3.00 **Funding Support:**
Project Contribution:
National Academy Member: N

ARTICLES:

Publication Type: Journal Article Peer Reviewed: Y **Publication Status:** 1-Published
Journal: Sensors
Publication Identifier Type: DOI Publication Identifier: 10.3390/s17102192
Volume: 17 Issue: 10 First Page #: 2192
Date Submitted: 8/29/18 12:00AM Date Published: 9/23/17 8:00AM
Publication Location:
Article Title: Drawing Sensors with Ball-Milled Blends of Metal-Organic Frameworks and Graphite
Authors: Michael Ko, Aylin Aykanat, Merry K. Smith and Katherine A. Mirica
Keywords: gas sensor; chemiresistor; metal-organic framework
Abstract: The synthetically tunable properties and intrinsic porosity of conductive metal-organic frameworks (MOFs) make them promising materials for transducing selective interactions with gaseous analytes in an electrically addressable platform. The implementation of these materials, however, is limited by the available methods for device incorporation due to their poor solubility and moderate electrical conductivity. This manuscript describes a straightforward method for the integration of moderately conductive MOFs into chemiresistive sensors by mechanical abrasion. To improve electrical contacts, blends of MOFs with graphite were generated using a solvent-free ball-milling procedure.
Distribution Statement: 3-Distribution authorized to U.S. Government Agencies and their contractors
Acknowledged Federal Support: **Y**

Publication Type: Journal Article Peer Reviewed: Y **Publication Status:** 1-Published
Journal: Journal of the American Chemical Society
Publication Identifier Type: DOI Publication Identifier: 10.1021/jacs.7b08840
Volume: Issue: First Page #:
Date Submitted: 8/29/18 12:00AM Date Published: 10/31/17 8:00AM
Publication Location:
Article Title: Self-Organized Frameworks on Textiles (SOFT): Conductive Fabrics for Simultaneous Sensing, Capture, and Filtration of Gases
Authors: Merry K. Smith, Katherine A. Mirica
Keywords: electronic sensors on textiles
Abstract: Wearable electronics have the potential to advance personalized health care, alleviate disability, enhance communication, and improve homeland security. Development of multifunctional electronic textiles (e-textiles) with the capacity to interact with the local environment is a promising strategy for achieving electronic transduction of physical and chemical information. This paper describes a simple and rapid approach for fabricating multifunctional e-textiles by integrating conductive two-dimensional (2D) metal–organic frameworks (MOFs) into fabrics through direct solution-phase self-assembly from simple molecular building blocks. These e-textiles display reliable conductivity, enhanced porosity, flexibility, and stability to washing. The functional utility of these integrated systems is demonstrated in the context of chemiresistive gas sensing, uptake, and filtration.
Distribution Statement: 3-Distribution authorized to U.S. Government Agencies and their contractors
Acknowledged Federal Support: **Y**

RPPR Final Report
as of 31-Aug-2021

Publication Type: Journal Article Peer Reviewed: Y **Publication Status:** 1-Published
Journal: ACS Applied Materials & Interfaces
Publication Identifier Type: DOI Publication Identifier: 10.1021/acsami.8b03956
Volume: 10 Issue: 22 First Page #: 19248
Date Submitted: 8/29/18 12:00AM Date Published: 5/1/18 12:00AM
Publication Location:
Article Title: Conductive Metal–Organic Frameworks as Ion-to-Electron Transducers in Potentiometric Sensors
Authors: Lukasz Mendecki, Katherine A. Mirica
Keywords: conductive metal?organic frameworks; electrochemical sensors; ion-selective electrode; ion-to-electron transduction; potentiometric sensors
Abstract: This paper describes an unexplored property of conductive metal–organic frameworks (MOFs) as ion-to-electron transducers in the context of potentiometric detection. Several conductive two-dimensional MOF analogues were drop-cast onto a glassy carbon electrode and then covered with an ion-selective membrane to form a potentiometric sensor. The resulting devices exhibited excellent sensing properties toward anions and cations, characterized by a near-Nernstian response and over 4 orders of magnitude linear range. Impedance and chronopotentiometric measurements revealed the presence of large bulk capacitance (204 ± 2 ?F) and good potential stability (drift of 11.1 ± 0.5 ?A/h). Potentiometric water test and contact angle measurements showed that this class of materials exhibited hydrophobicity and inhibited the formation of water layer at the electrode/membrane interface, resulting in a highly stable sensing response with a potential drift as low as 11.1 ? A/h.
Distribution Statement: 3-Distribution authorized to U.S. Government Agencies and their contractors
Acknowledged Federal Support: **Y**

Publication Type: Journal Article Peer Reviewed: Y **Publication Status:** 1-Published
Journal: Chemical Communications
Publication Identifier Type: DOI Publication Identifier: 10.1039/C8CC02871K
Volume: 54 Issue: 57 First Page #: 7873
Date Submitted: 8/29/18 12:00AM Date Published:
Publication Location:
Article Title: Conductive two-dimensional metal–organic frameworks as multifunctional materials
Authors: Michael Ko, Lukasz Mendecki, Katherine A. Mirica
Keywords: metal-organic frameworks, multifunctional materials, 2018 Emerging Investigators
Abstract: Two-dimensional (2D) conductive metal–organic frameworks (MOFs) have emerged as a unique class of multifunctional materials due to their compositional and structural diversity accessible through bottom-up self-assembly. This feature article summarizes the progress in the development of 2D conductive MOFs with emphasis on synthetic modularity, device integration strategies, and multifunctional properties. Applications spanning sensing, catalysis, electronics, energy conversion, and storage are discussed. The challenges and future outlook in the context of molecular engineering and practical development of 2D conductive MOFs are addressed.
Distribution Statement: 3-Distribution authorized to U.S. Government Agencies and their contractors
Acknowledged Federal Support: **Y**

RPPR Final Report
as of 31-Aug-2021

Publication Type: Journal Article Peer Reviewed: Y **Publication Status:** 1-Published
Journal: Chemistry of Materials
Publication Identifier Type: DOI Publication Identifier: 10.1021/acs.chemmater.8b03897
Volume: Issue: First Page #:
Date Submitted: 1/25/19 12:00AM Date Published: 1/7/19 5:00AM
Publication Location:
Article Title: Proton Conduction in 2D Aza-Fused Covalent Organic Frameworks
Authors: Zheng Meng, Aylin Aykanat, Katherine A. Mirica
Keywords: proton transport; covalent organic frameworks
Abstract: This paper describes the first demonstration of a general concept for achieving facile proton conduction within a class of layered two-dimensional aza-fused ?-conjugated covalent organic frameworks (COFs). The built-in phenanthroline moieties promote efficient adsorption of water and acidification by H3PO4 to produce excellent proton conductivities of 10^(–5) and 10^(–3) S/cm for the pristine and acidified analogues, respectively. These molecular design concepts are poised for development of highly stable proton-conducting materials.
Distribution Statement: 3-Distribution authorized to U.S. Government Agencies and their contractors
Acknowledged Federal Support: **Y**

Publication Type: Journal Article Peer Reviewed: Y **Publication Status:** 1-Published
Journal: Chemical Reviews
Publication Identifier Type: DOI Publication Identifier: 10.1021/acs.chemrev.8b00311
Volume: 119 Issue: 1 First Page #: 478
Date Submitted: 1/25/19 12:00AM Date Published: 1/3/19 5:00AM
Publication Location:
Article Title: Electrically-Transduced Chemical Sensors Based on Two-Dimensional Nanomaterials
Authors: Zheng Meng, Robert M. Stolz, Lukasz Mendecki, Katherine A. Mirica
Keywords: chemical sensors; 2D nanomaterials
Abstract: Electrically–transduced sensors, with their simplicity and compatibility with standard electronic technologies, produce signals that can be efficiently acquired, processed, stored, and analyzed. Two dimensional (2D) nanomaterials, including graphene, phosphorene (BP), transition metal dichalcogenides (TMDCs), and others, have proven to be attractive for the fabrication of high–performance electrically-transduced chemical sensors due to their remarkable electronic and physical properties originating from their 2D structure. This review highlights the advances in electrically-transduced chemical sensing that rely on 2D materials. The structural components of such sensors are described, and the underlying operating principles for different types of architectures are discussed. The structural features, electronic properties, and surface chemistry of 2D nanostructures that dictate their sensing performance are reviewed. Key advances in the application of 2D materials, from both a historical
Distribution Statement: 3-Distribution authorized to U.S. Government Agencies and their contractors
Acknowledged Federal Support: **Y**

RPPR Final Report
as of 31-Aug-2021

Publication Type: Journal Article Peer Reviewed: Y **Publication Status:** 1-Published
Journal: Journal of the American Chemical Society
Publication Identifier Type: DOI Publication Identifier: 10.1021/jacs.8b11257
Volume: Issue: First Page #:
Date Submitted: 1/25/19 12:00AM Date Published: 1/25/19 10:00AM
Publication Location:
Article Title: Welding Metallophthalocyanines into Bimetallic Molecular Meshes for Ultrasensitive, Low-Power Chemiresistive Detection of Gases
Authors: Zheng Meng, Aylin Aykanat, Katherine A. Mirica
Keywords: metal-organic frameworks, gas sensors
Abstract: This paper describes the first demonstration of using a series of isoreticular nickel phthalocyanine- and nickel naphthalocyanine-based bimetallic conductive two-dimensional (2D) metal–organic frameworks (MOFs) as active materials in chemiresistive sensing of gases. Devices achieve exceptional sensitivity at sub-part-per-million (ppm) to part-per-billion (ppb) detection limits toward NH3 (0.31–0.33 ppm), H2S (19–32 ppb), and NO (1.0–1.1 ppb) at low driving voltages (0.01–1.0 V) within 1.5 min of exposure. The devices maintain their performance in the presence of humidity (5000 ppm of H2O). The isoreticular analogs enable modular control over selectivity and sensitivity in gas sensing through different combinations of linkers and metal nodes. Electron paramagnetic resonance spectroscopy and X-ray photoelectron spectroscopy studies suggest that the chemiresistive response of the MOFs involves charge transfer interactions triggered by the analytes adsorbed on MOFs.
Distribution Statement: 3-Distribution authorized to U.S. Government Agencies and their contractors
Acknowledged Federal Support: **Y**

Publication Type: Journal Article Peer Reviewed: Y **Publication Status:** 1-Published
Journal: Journal of the American Chemical Society
Publication Identifier Type: DOI Publication Identifier: 10.1021/jacs.9b03441
Volume: 141 Issue: 30 First Page #: 11929
Date Submitted: 8/30/19 12:00AM Date Published: 6/1/19 4:00AM
Publication Location:
Article Title: Two-Dimensional Chemiresistive Covalent Organic Framework with High Intrinsic Conductivity
Authors: Zheng Meng, Robert M. Stolz, Katherine A. Mirica
Keywords: covalent organic frameworks
Abstract: This paper describes the synthesis of a novel intrinsically conductive two-dimensional (2D) covalent organic framework (COF) through the aromatic annulation of 2,3,9,10,16,17,23,24-octa-aminophthalocyanine nickel(II) and pyrene-4,5,9,10-tetraone. The intrinsic bulk conductivity of the COF material (termed COF-DC-8) reached 2.51 × 10–3 S/m, and increased by 3 orders of magnitude with I2 doping. Electronic calculations revealed an anisotropic band structure, with the possibility for significant contribution from out-of-plane charge-transport to the intrinsic bulk conductivity. Upon integration into chemiresistive devices, this conductive COF showed excellent responses to various reducing and oxidizing gases, including NH3, H2S, NO, and NO2, with parts-per-billion (ppb) limits of detection (for NH3 = 70 ppb, for H2S = 204 ppb, for NO = 5 ppb, and for NO2 = 16 ppb based on 1.5 min exposure). Electron paramagnetic resonance spectroscopy and X-ray photoelectron spectroscopy studies suggested
Distribution Statement: 3-Distribution authorized to U.S. Government Agencies and their contractors
Acknowledged Federal Support: **Y**

CONFERENCE PAPERS:

Publication Type: Conference Paper or Presentation **Publication Status:** 1-Published
Conference Name: North Eastern Section of the American Chemical Society
Date Received: 29-Aug-2018 Conference Date: 05-Oct-2017 Date Published: 05-Oct-2017
Conference Location: Milford, MA
Paper Title: Multifunctional Materials for Chemical Sensing and Microelectronics
Authors: Katherine A. Mirica
Acknowledged Federal Support: **Y**

RPPR Final Report
as of 31-Aug-2021

Publication Type: Conference Paper or Presentation **Publication Status:** 0-Other
Conference Name: Sigma Xi Seminar at U.S. Army Natick Soldier Research
Date Received: 29-Aug-2018 Conference Date: 13-Nov-2017 Date Published:
Conference Location: Natick, MA
Paper Title: Multifunctional Materials for Chemical Sensing and Microelectronics
Authors: Katherine A. Mirica
Acknowledged Federal Support: **Y**

Publication Type: Conference Paper or Presentation **Publication Status:** 0-Other
Conference Name: Advanced Materials for Energy and Bioengineering Applications (AMEBA) Symposium
Date Received: 29-Aug-2018 Conference Date: 04-Dec-2017 Date Published: 04-Dec-2017
Conference Location: Burlington, VT
Paper Title: Stimuli-Responsive Materials for Chemical Sensing and Gas Capture
Authors: Katherine A. Mirica
Acknowledged Federal Support: **Y**

Publication Type: Conference Paper or Presentation **Publication Status:** 0-Other
Conference Name: 4. 2nd From Carbon-Rich Molecules to Carbon-Based Materials Conference
Date Received: 29-Aug-2018 Conference Date: 08-Jun-2018 Date Published: 08-Jun-2018
Conference Location: Nassau, Bahamas
Paper Title: Porous Scaffolds for Electronically-Transduced Chemical Sensing and Capture
Authors: Katherine A. Mirica
Acknowledged Federal Support: **Y**

PATENTS:

Intellectual Property Type: Patent Date Received: **30-Aug-2018**
Patent Title: Conductive Textiles and Uses Thereof in Functional Devices
Patent Abstract: This application claims priority to U.S. Provisional Patent Application No. 62/489,851, filed on Ap
Patent Number: 15/962,156
Patent Country: USA
Application Date: 25-Apr-2018 Application Status: 2
Date Issued:

Intellectual Property Type: Patent Date Received: **30-Aug-2018**
Patent Title: Metal-Organic Frameworks as Ion-to-Electron Transducers and Detectors
Patent Abstract: This invention describes the use of conductive metal-organic frameworks as ion-to-electron tran
Patent Number: 18/46,510
Patent Country: USA
Application Date: 13-Aug-2018 Application Status: 2
Date Issued:

Intellectual Property Type: Patent Date Received: **30-Aug-2018**
Patent Title: Formation of Metal-Organic Frameworks
Patent Abstract: This invention describes a new method for growing metal-organic frameworks using metallized s
Patent Number: 62/681,436
Patent Country: USA
Application Date: 06-Jun-2018 Application Status: 1

RPPR Final Report
as of 31-Aug-2021

Date Issued:

Intellectual Property Type: Patent Date Received: **30-Aug-2018**
Patent Title: Conductive Metal-Organic Frameworks for Voltammetric Detection of Neurochemicals
Patent Abstract: This invention describes the use of conductive metal-organic frameworks as working electrodes
Patent Number: 62/688,261
Patent Country: USA
Application Date: 21-Jun-2018 Application Status: 1
Date Issued:

Intellectual Property Type: Patent Date Received: **30-Aug-2019**
Patent Title: Two-dimensional Stimuli-Response Covalent Organic Frameworks with High Intrinsic Conductivity
Patent Abstract: This paper describes the synthesis of a novel intrinsically
Patent Number: 62/837,118
Patent Country: USA
Application Date: 22-Apr-2019 Application Status: 1
Date Issued:

Intellectual Property Type: Patent Date Received: **30-Aug-2019**
Patent Title: Conductive Bimetallic Metal-Organic Frameworks for the Detection of Analytes
Patent Abstract: This application describes the first demonstration of using a series of isoreticular nickel phthaloc
Patent Number: 62/719,264
Patent Country: USA
Application Date: 17-Aug-2018 Application Status: 1
Date Issued:

Partners

,

We have established a collaboration with Gregory Peterson (Aberdeen Proving Ground, MD) related to this project.

I certify that the information in the report is complete and accurate:
Signature: Katherine Mirica
Signature Date: 8/31/21 12:20PM

1) Major activities:

- Molecular Design of Receptors
- Molecular Design of Stimuli-Responsive Materials
- Design and Synthesis of Stimuli-Responsive MOFs
- Design and Synthesis of Stimuli-Responsive COFs
- Studies of Electrical Properties of MOFs and COFs
- Studies of Magnetic Properties of MOFs and COFs
- Coupling Chemiresistance with Magnetoresistance

2) Specific objectives:

- Computational assessment of analyte-MOF and analyte-COF interactions
- Optimization of morphological control for producing free-standing MOF nanowires and nanosheets
- Synthesis and characterization of COF precursors
- Measurements of conductivity of MOFs having highly tuned morphological control
- Examination of the impact of the electrodes on device performance in MOFs
- EPR and SQUID magnetometry studies of MOFs
- Fabrication of setup for measuring magnetoresistance

3) Significant results: see below

Figure 1. Progress towards Task 1.1.1. Computational modeling of host sites reveals analyte-specific binding modes and energies. Shown are the computationally modeled interaction of Ni-bis(dioxolene) host-sites with analyte guests of NO and NH_3. Ni-bis(dioxolene) binds NO favorably by 23.4 kcal/mol. The binding event does not interfere with the ligand-metal-ligand planarity. The interaction of NH_3 with Ni-bis(dioxolene) is favorable by 11.9 kcal/mol. Binding NH_3 causes the Ni to pucker out of the plane of the ligands. Hydration of the axial position of Ni-bis(dioxolene) host-sites causes it react as a Brønsted acid host site rather than a Lewis acid site. The change in acidity causes a more favorable host-guest interaction with ammonia by more than 20 kcal/mol.

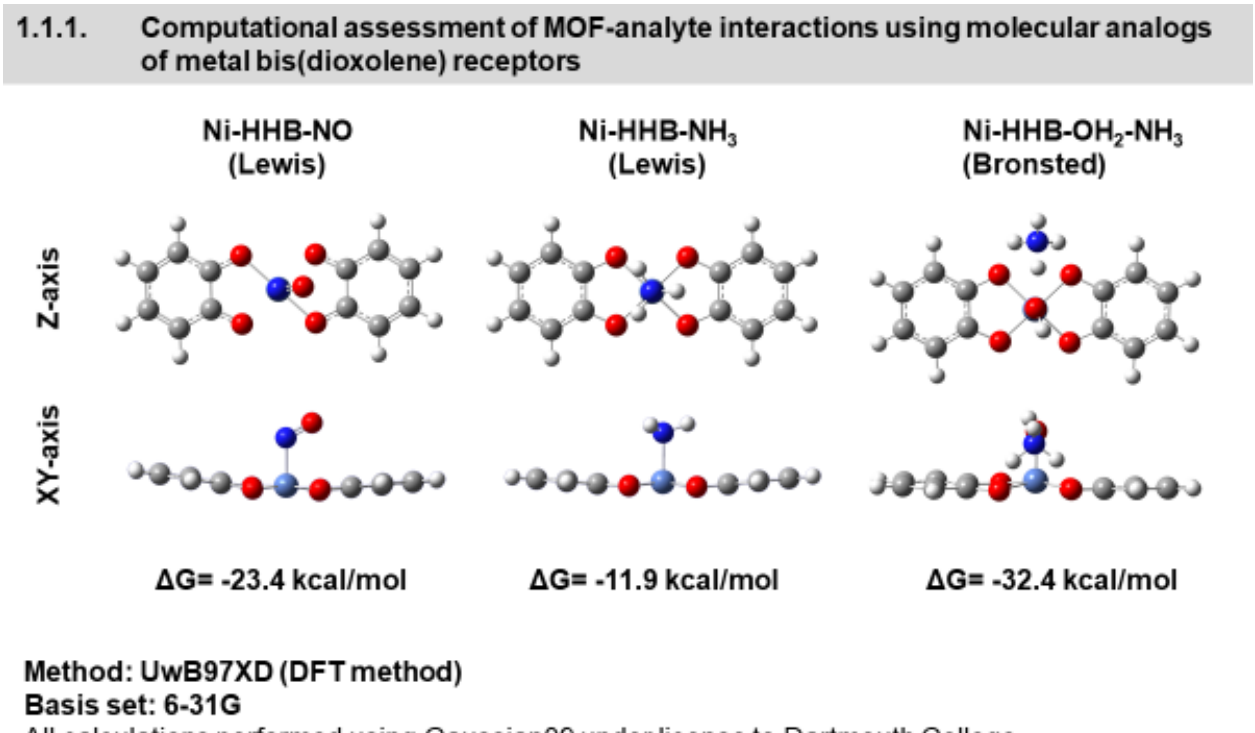

Figure 2. Progress towards Task 1.1.1. Computational modelling of acidic site interactions between NH_3 and various MOFs demonstrates the stability of all binding modalities but a preference for adsorption to Brønsted acid interactions. The advancement in modelling full HHTP molecules instead of fractional ligands is expected to drastically improve calculation accuracy.

1.1.1. Computational assessment of MOF-analyte edge-type interactions using molecular analogs of metal bis(dioxolene) receptors

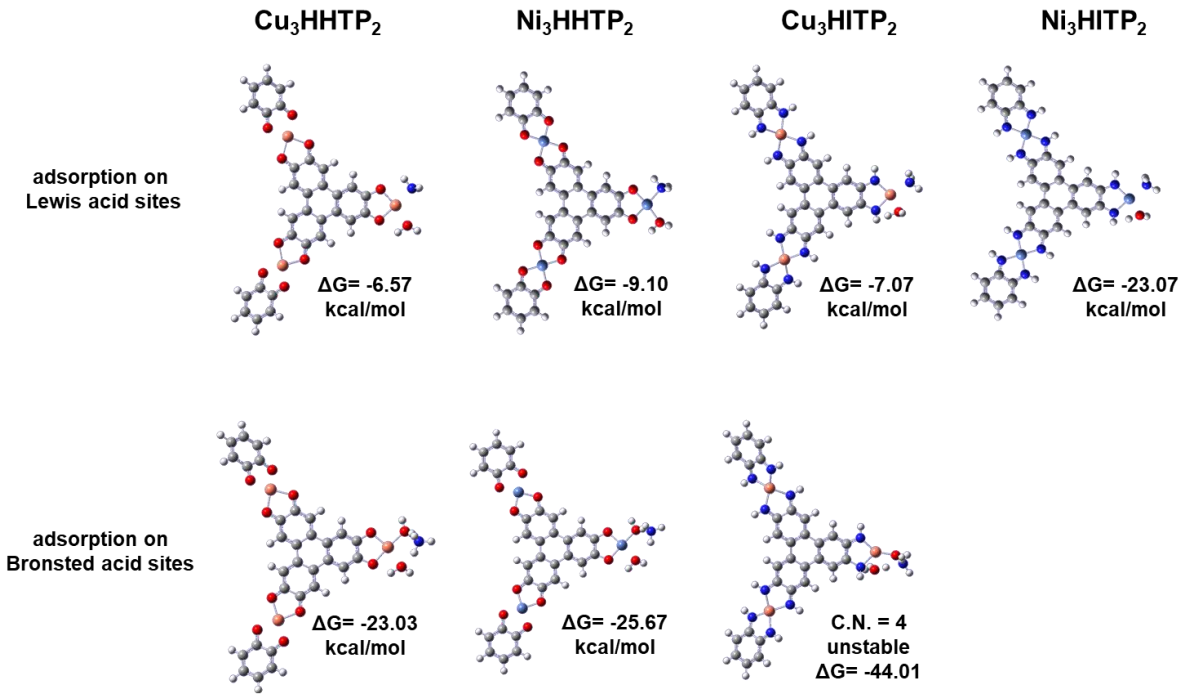

Method: UwB97XD (DFT method)
Basis set: 6-31G
All calculations performed using Gaussian09 under license to Dartmouth College

Figure 3. Progress towards Task 1.1.2. The Host–Guest interactions between MPc-Pyr-COFs and targeted gas analytes was examined using computational DFT techniques. The most favorable adsorption location was determined for two types of gases. Representative adsorption geometries are shown for **a)** diatomic electron withdrawing gases including NO, CO, and O_2, and **b)** highly reduced electron donating gases NH_3, H_2O, and H_2S. The most favorable host site was determined for each MPc-Pyr COF + gas pair to be the vacant axial coordination site of the MPc metal. The table **c)** shows calculated adsorption energy of MPc-Pyr-COF (M=Fe, Co, Ni, Cu) and gases (NO, CO, O_2, NH_3, H_2O, and H_2S). Adsorption sites were found using the Adsorption-Anneal locator in Materials Studio 2019. The most favorable adsorption location determined by Adsorption-Anneal was then optimized using DMol3 as part of Materials Studio 2019. Optimized geometries, single point energies, and physical/electronic parameters were modelled using the M11-L method and a DNP basis set.

1.1.2 Computational assessment of Host-Guest interactions MPc-Pyr-COFs and gasotransmitters (M = Fe, Co, Ni, Cu)

a)

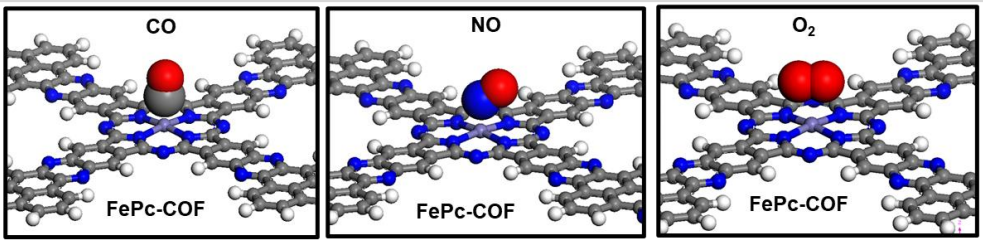

b)

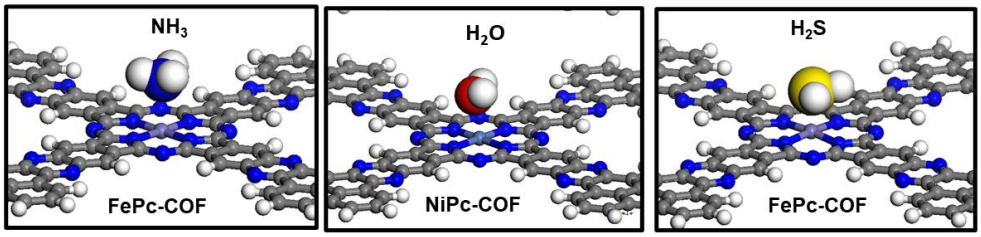

c)

E_{ads} (kcal/mol)	FePc-Pyr	CoPc-Pyr	NiPc-Pyr	CuPc-Pyr
CO	-102.7	-80.4	-13.9	-32.1
NO	-91.2	-11.6	-3.3	-55.8
O_2	-68.2	5.3	8.2	-
NH_3	-106.0	-80.7	-15.4	-12.7
H_2S	-83.4	-63.2	-62.4	-59.4
H_2O	-86.1	-18.1	-61.5	-55.1

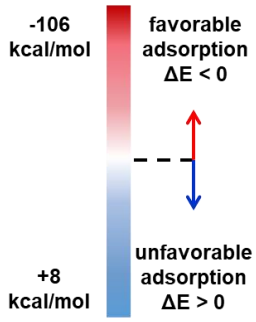

Figure 4. Progress towards Task 1.2.1. Synthetic scheme implemented for generating the proposed M_3HHTP_2 MOFs (M=Fe, Co, Ni, Cu). Electronic band structure for (A) $Fe_3(HHTP)_2$, (B) $Co_3(HHTP)_2$, (C) $Ni_3(HHTP)_2$, and (D) $Cu_3(HHTP)_2$ calculated by CASTEP imbedded in Materials Studio 2017 (cutoff energy: 300-500 eV; k-point mesh: 2×2×3).

1.2.1. Computational examination of the influence of metal and ligand on band gap of MOFs monolayers

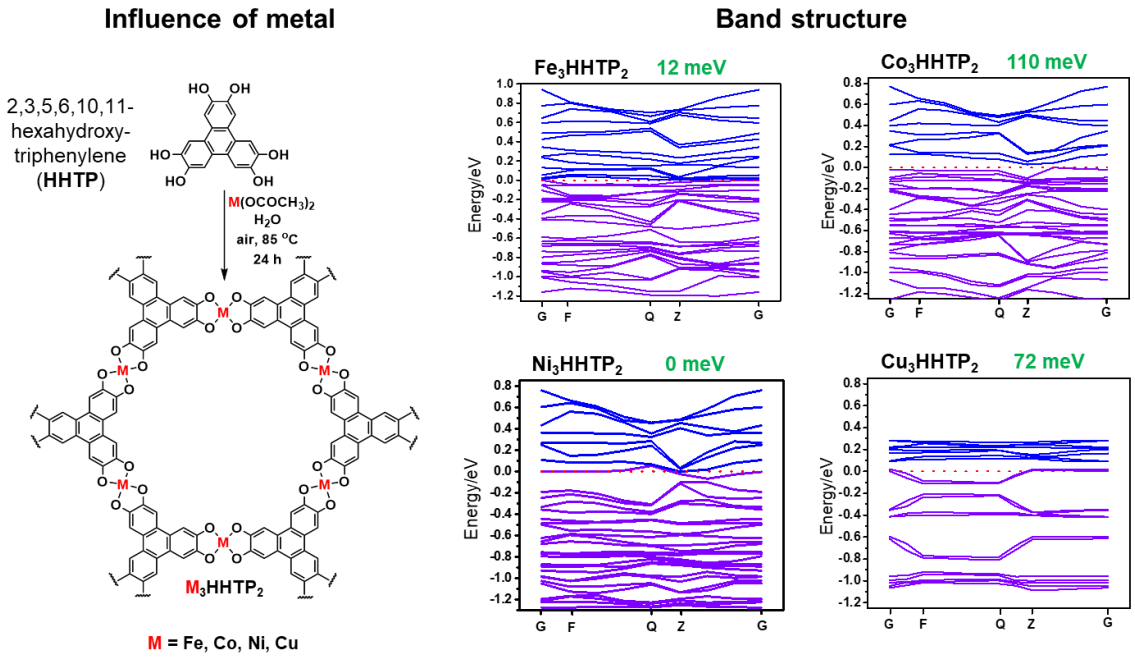

Figure 5. Progress towards Task 1.2.2. Calculated electronic band structure (left side) and density of state (right side) for bulk MPc-Pyr COFs (M=Fe, Co, Ni, Cu) having an eclipsed stacking structure. Geometry optimizations and property modelling was done using CASTEP as part of materials studio 2019 (cutoff energy: 300-500 eV; k-point mesh: 2×2×3). The GGA functional PBE was used. A Hubbard correction of 3.0 eV was used for all metal ions.

1.2.2. Computational examination of the influence of metal and ligand on band gap of MPc-COFs (M = Fe, Co, Ni, Cu)

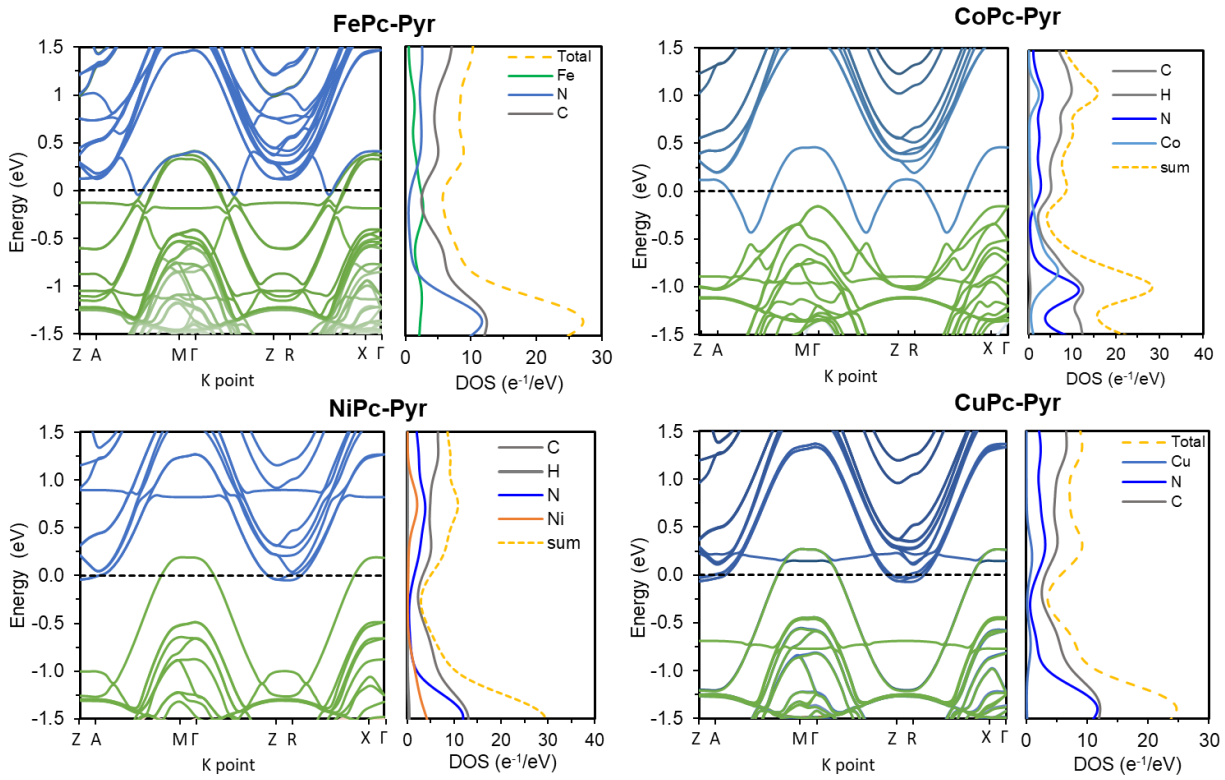

Figure 6. Progress towards Task 1.2.2.a Calculated electronic band structure for monolayers of MPc-Pyr (M=Fe, Co, Ni, Cu). A bandgap was observed for the monolayer models in contrast to the lack of bandgap observed for the bulk material calculations. Geometry optimizations and property modelling was done using CASTEP as part of materials studio 2019 (cutoff energy: 300-500 eV; k-point mesh: 2×2×3). The GGA functional PBE was used. A Hubbard correction of 3.0 eV was used for all metals.

1.2.2 Computational examination of MPc-COF monolayers (M = Fe, Co, Ni, Cu)

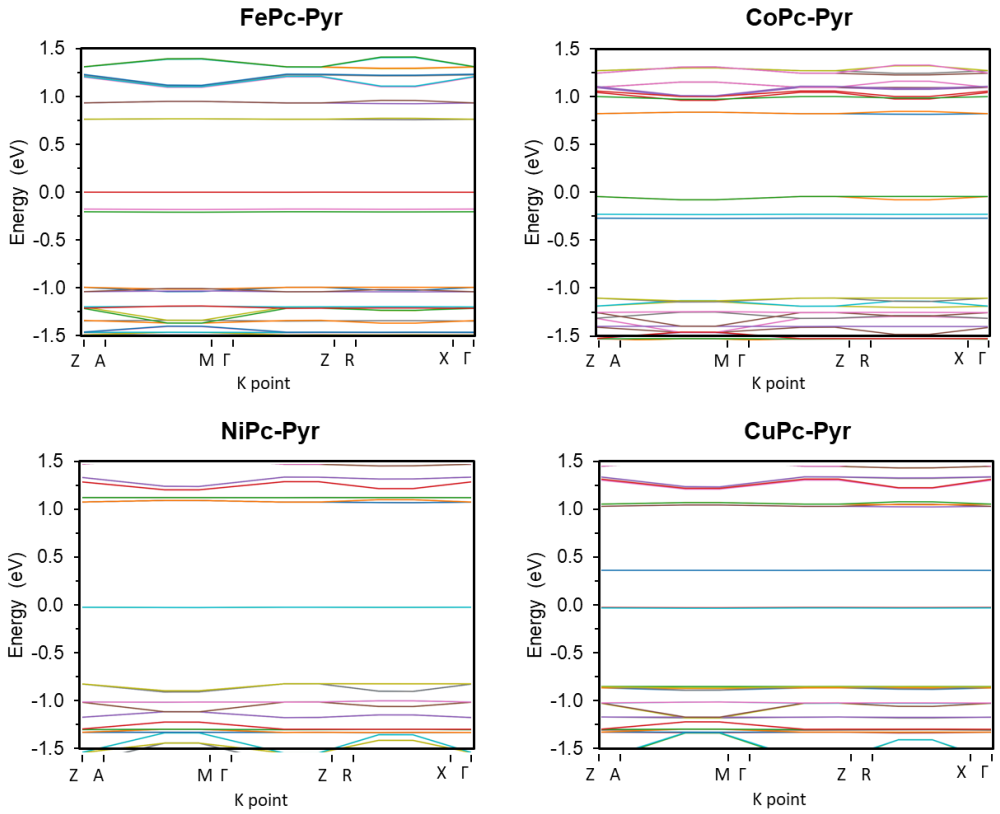

Figure 7. Progress towards Task 1.3.1. Scanning electron micrographs showing that control over synthetic conditions (conditions in table below) enables morphological tuning of layered MOF-based nanostructures through solvothermal synthesis.

1.3.1. Optimization of morphological control for producing free-standing MOF nanowires and nanosheets

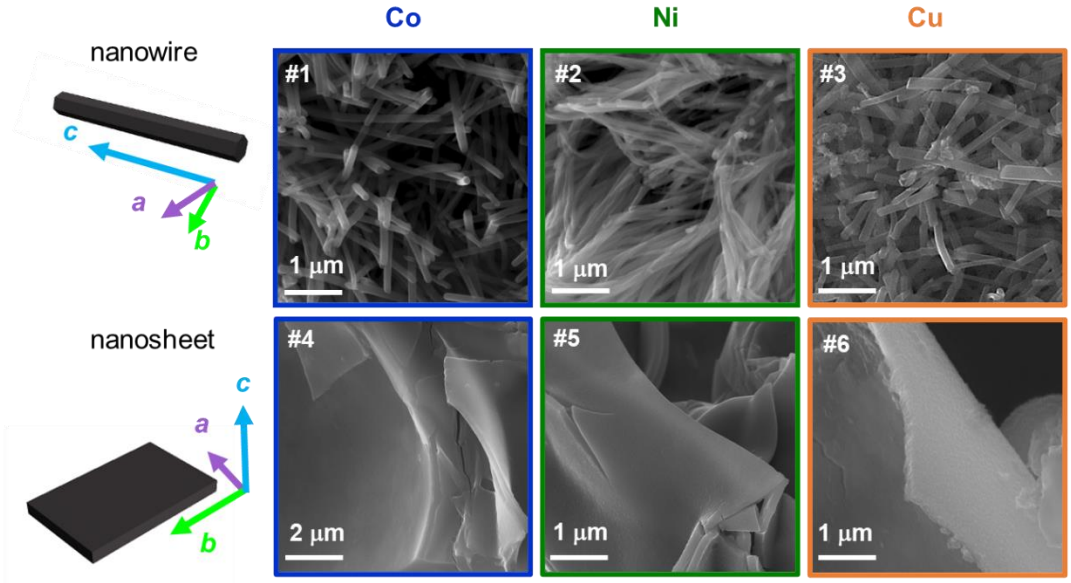

synthetic conditions

nanowires			
M	solvent	diameter	#
Co	H_2O	88 ± 23 nm	1
Ni	H_2O	85 ± 47 nm	2
Cu	H_2O	73 ± 31 nm	3

nanosheets			
M	solvent	thickness	#
Co	H_2O/Et_2O	540 ± 50 nm	4
Ni	H_2O[a]	184 ± 66 nm	5
Cu	H_2O/Et_2O	150 ± 30 nm	6

[a] slow addition

Figure 8. Progress towards Task 1.3.1. Powder X-Ray crystallography (pXRD) analysis confirms the structures of MOFs. Exfoliation of nanowire-based nanostructures by sonication enables visualization of the layered morphology by transmission electron microscopy (TEM).

1.3.1 Optimization of morphological control for producing free-standing MOF nanowires and nanosheets

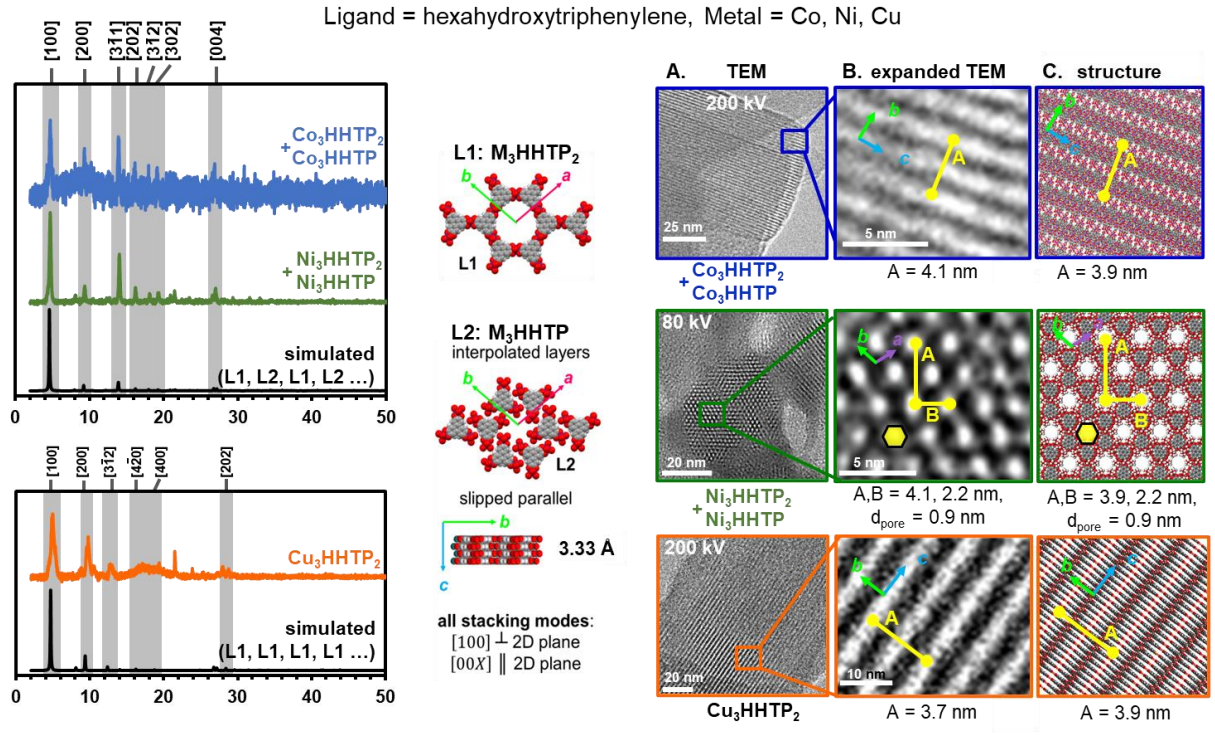

Figure 9. Progress towards Task 1.3.2-3 Calculated electronic band structure (left) and density of state (right) for **a)** CoPc-Cu-NH, **b)** CoPc-Cu-O MOFs, **c)** NiPc-Cu-NH, and **d)** NiPc-Cu-O, **e)** NiPc-Ni-O, and **f)** Corresponding first Brillouin zone and high-symmetry K-points.

1.3.2 Computational assessment of the influence of metal and ligand on the anisotropy of charge transport in bimetallic MOFs

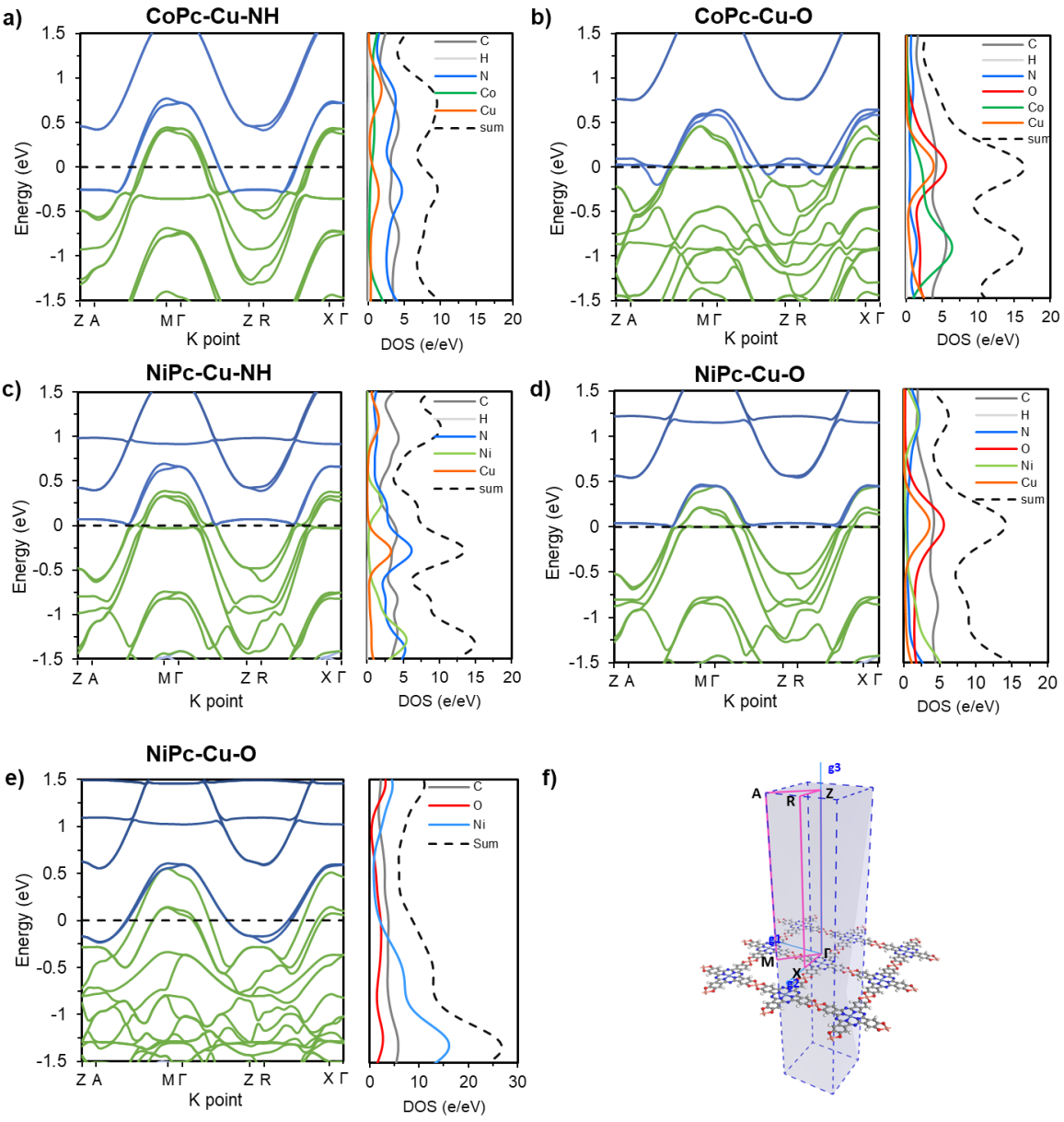

Figure 10. Progress towards Task 1.4.1. Synthetic scheme implemented to produce the proposed COF building blocks metal octaaminophthalocyanine (M = Fe, Co, Ni, Cu). The synthetic strategy, and resulting yields are shown.

1.4.1. Synthesis and Characterization of COF precurors

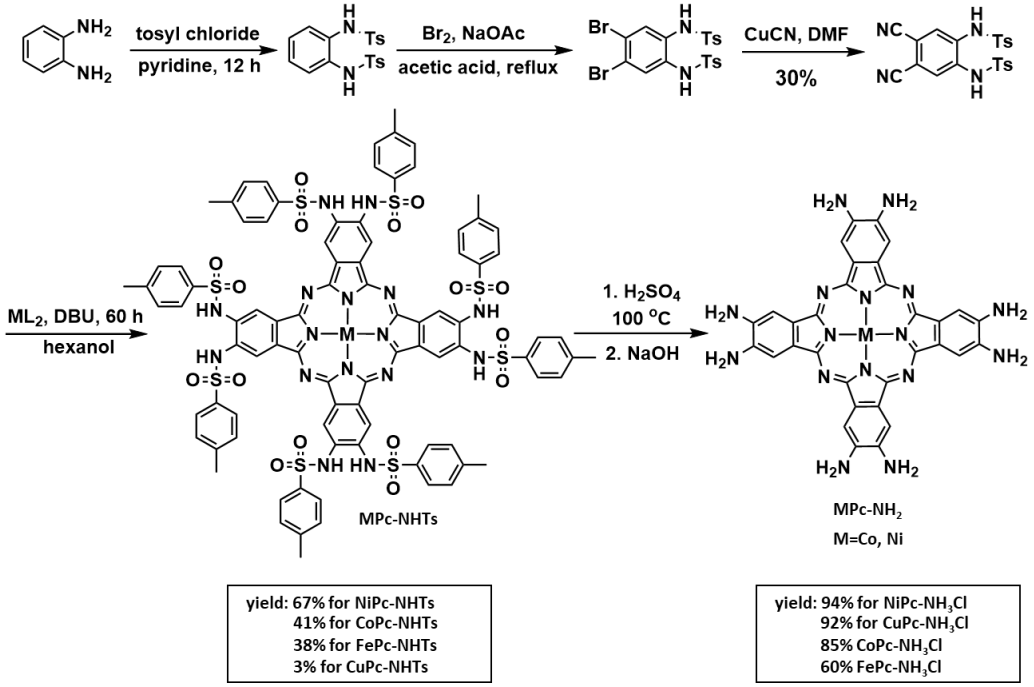

Figure 11. Progress towards Task 1.4.1. Characterization of ligand precursors for the MPc-Pyr COF was performed with H^1-NMR (acetone-d_6, 300 MHz).

1.4.1 H^1-NMR characterization of paramagnetic MPc-Pyr COF precursors

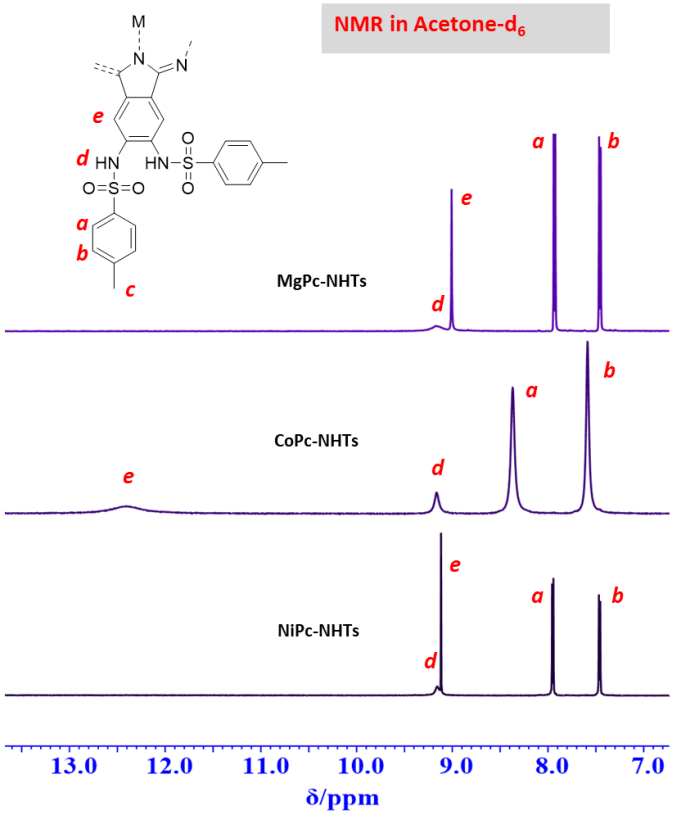

Figure 12. Progress towards Task 1.4.1.b Characterization of ligand precursors for the MPc-Pyr COF by HRMS (TOF ES+). The parent peaks are labeled with their M/z values where M is the molecular weight of the analyzed compound.

1.4.1 HRMS characterization of FePc-Pyr and CoPc-Pyr COF precursors

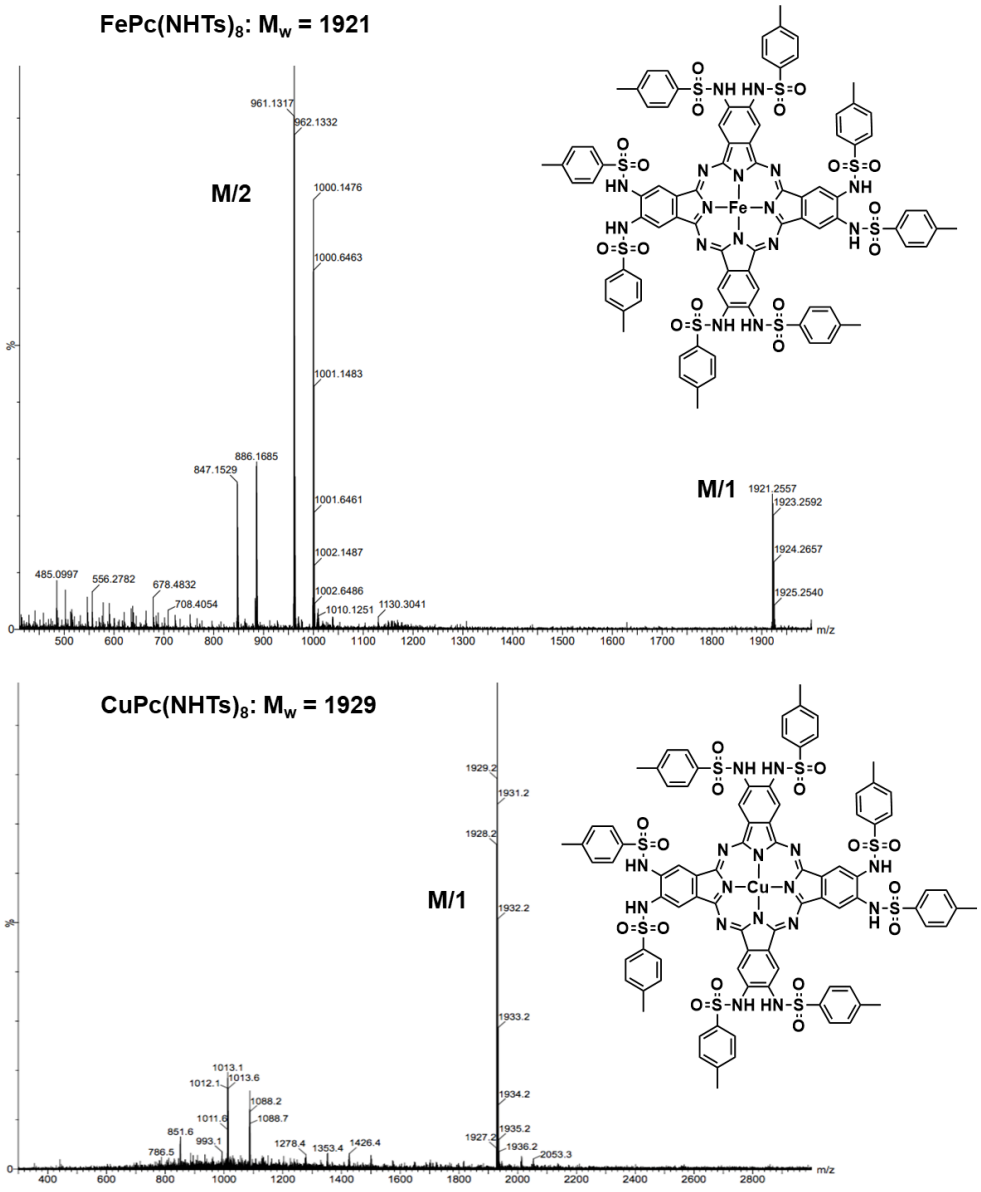

Figure 13. Progress towards Task 1.4.2. a) Synthetic scheme for conductive COF, named NiPc-Pyr. Structural characterization: **b)** Top and side view of the structure of M-COF-DC-8 with 2 × 2 square grids in eclipsed stacking mode with a Lieb lattice. **c)** Comparison of the simulated and experimental PXRD patterns. **d)** SEM and TEM characterization of M-COF-DC-8 crystalline powders.

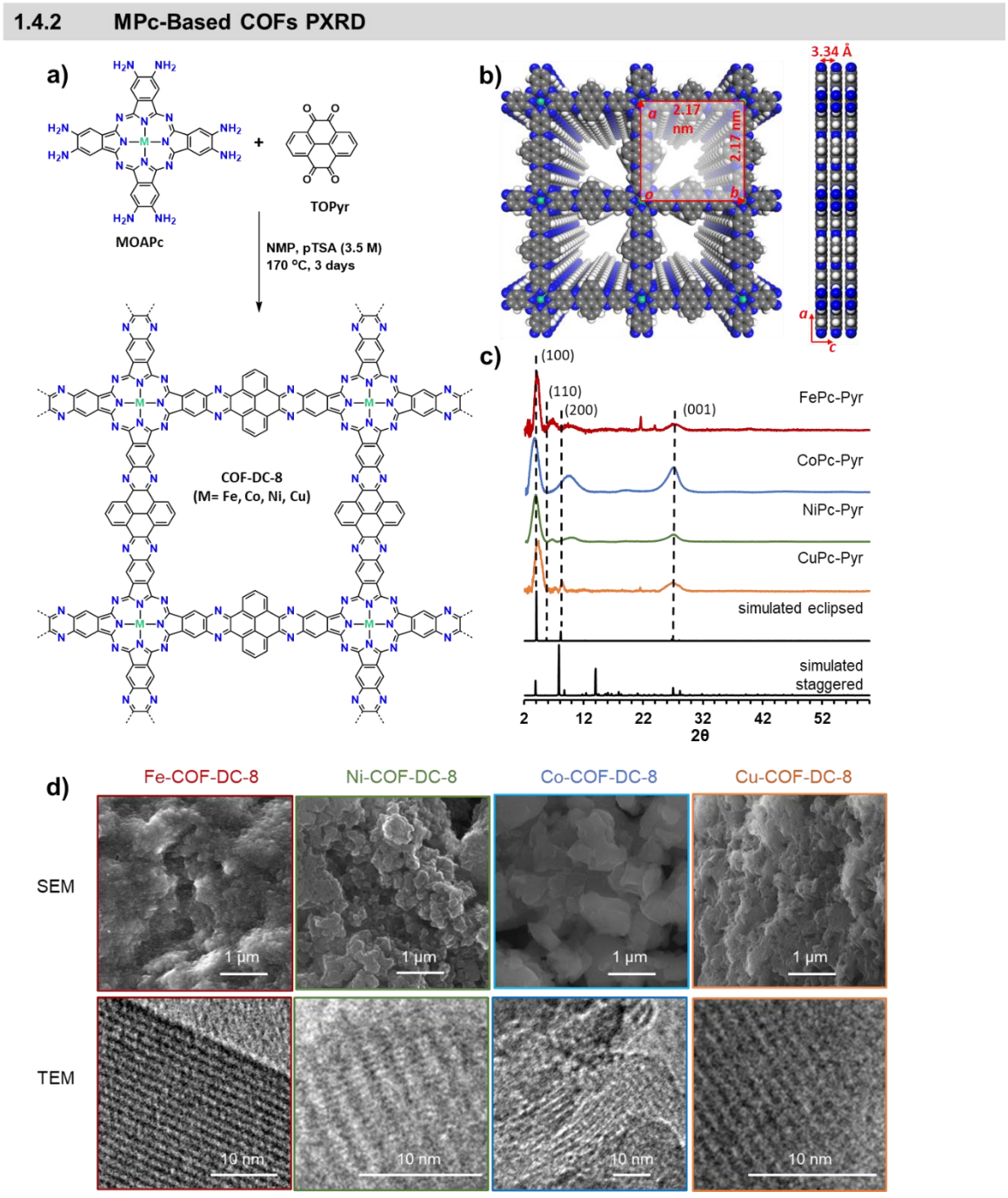

Figure 14. Progress towards Task 1.4.2. BET surface area analysis of the Ni-COPF-DC-8 COF. **a)** BET isotherm measured with N_2. **b)** Quantity adsorbed versus thickness for Ni-COF-DC-8. (c) Isotherm and BET surface area of Fe-COF-DC-8. (d) Isotherm and BET surface area of Co-COF-DC-8. (e) Isotherm and BET surface area of Ni-COF-DC-8. (f) Isotherm and BET surface area of Cu-COF-DC-8. Further optimization is needed to maximize specific surface area for selected COFs.

1.4.2 BET characterization of MPc-based COFs

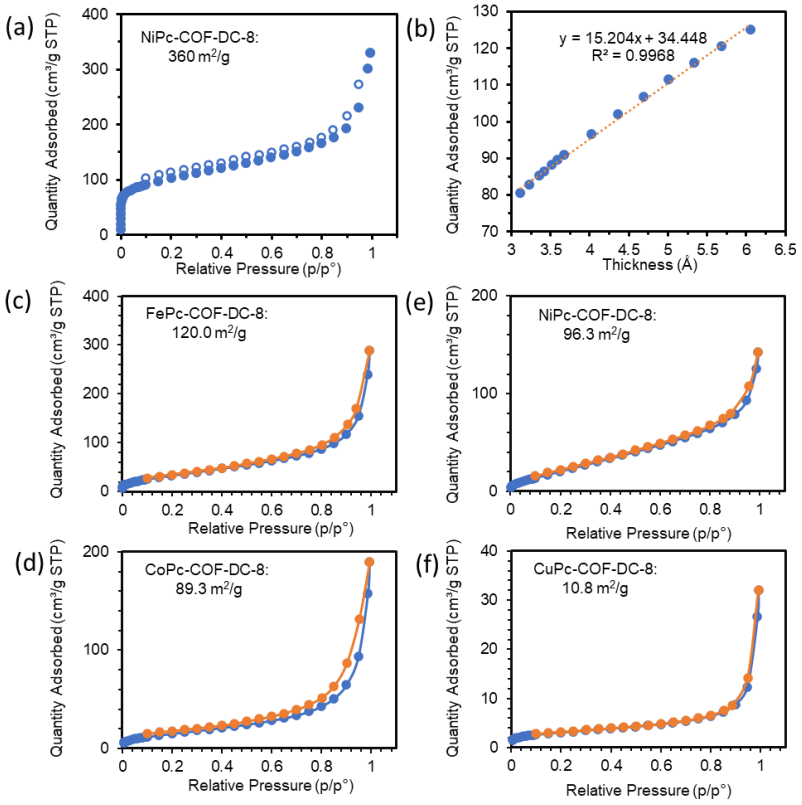

Figure 15. Progress towards Task 1.4.3. SEM obtained for NiPc-Pyr under different conditions which showed (a) flake, (b) rod and (c) grain like morphology.

1.4.3. Morphological control within MPc-based COFs

Entry	solvent	[NiOAPc] /mM	additives	Temperature /°C	time
A	DCB/DMAC (1/1)	2	--	202	10 d
B	DCB/DMAC (1/1)	2	H_2SO_4 (9 eq)	202	10 d
C	NMP/6 M HOAc (1/0.25)	2	--	200	7 d

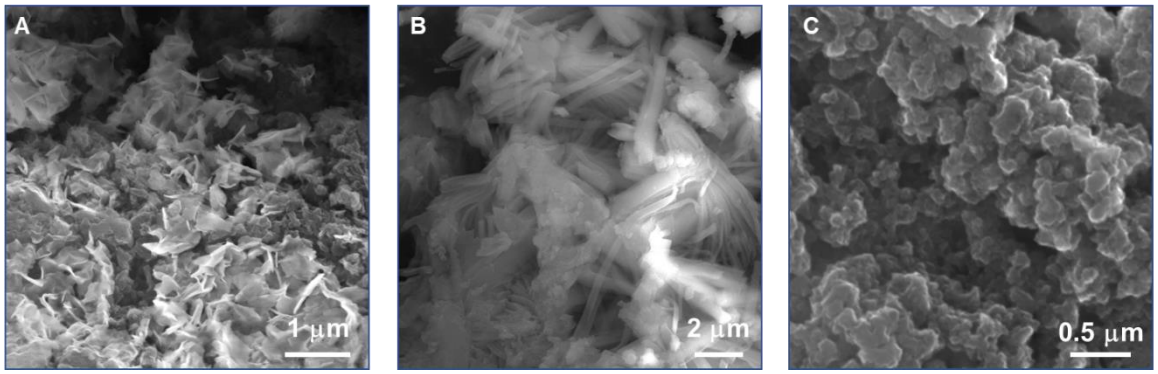

Figure 16. Progress towards Task 2.1.1. Images of M_3HHTP_2 (M=Cu, Ni, Co) thin films positioned in chemiresistive devices. Change in conductance over time plots reveals the normalized response of MOFs towards analytes.

2.1.1. Measurement of conductivity of MOFs having highly tuned morphological control

Preliminary Results for Chemiresistive Detection of Gases Using Thin Films

M_3HHTP_2 Film Glass Slides

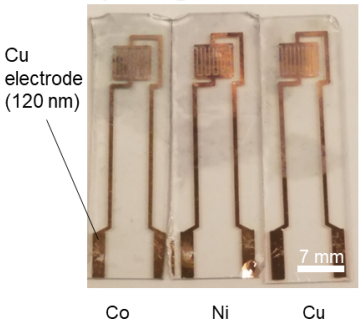

Washing Conditions:

1. Submerge in H_2O for 12 hours
   - Air dry
2. Submerge in acetone for 12 hours
   - Air dry

Devices*	Cu_3HHTP_2 (MΩ)	Ni_3HHTP_2 (MΩ)	Co_3HHTP_2 (MΩ)
(1)	1.26	12.98	16.32
(2)	10.26	1.03	30.96
(3)	-	2.60	2.90

*device yield 80% after the washing process

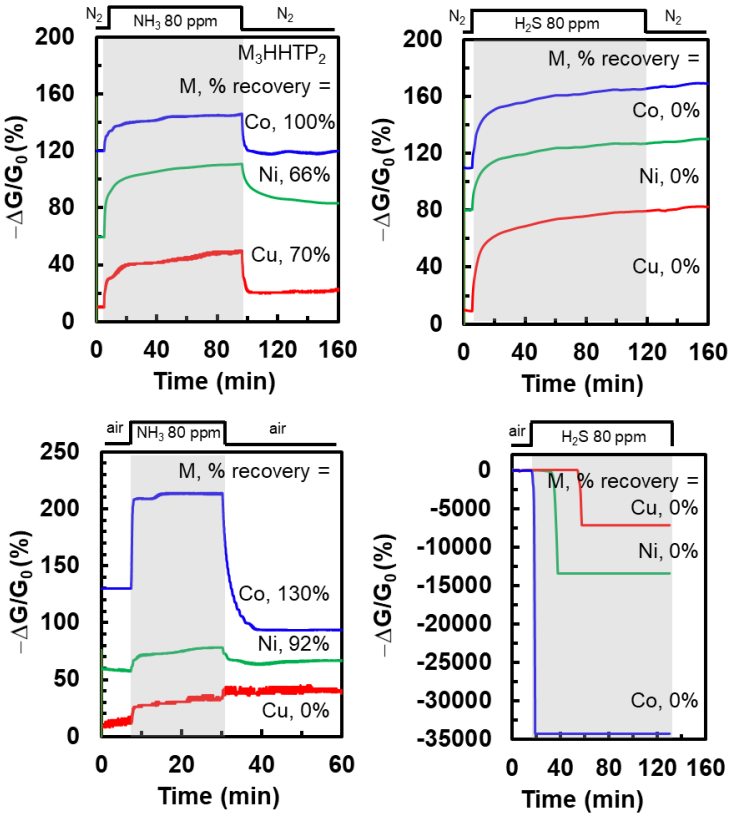

Figure 17. Progress towards Task 2.1.2. MOF chemiresistors fabricated using Langmuir-Schaefer deposition. The response of the MOFs towards analytes reveals the change in normalized conductance over time plots and signal to noise ratios as a function of electrode type.

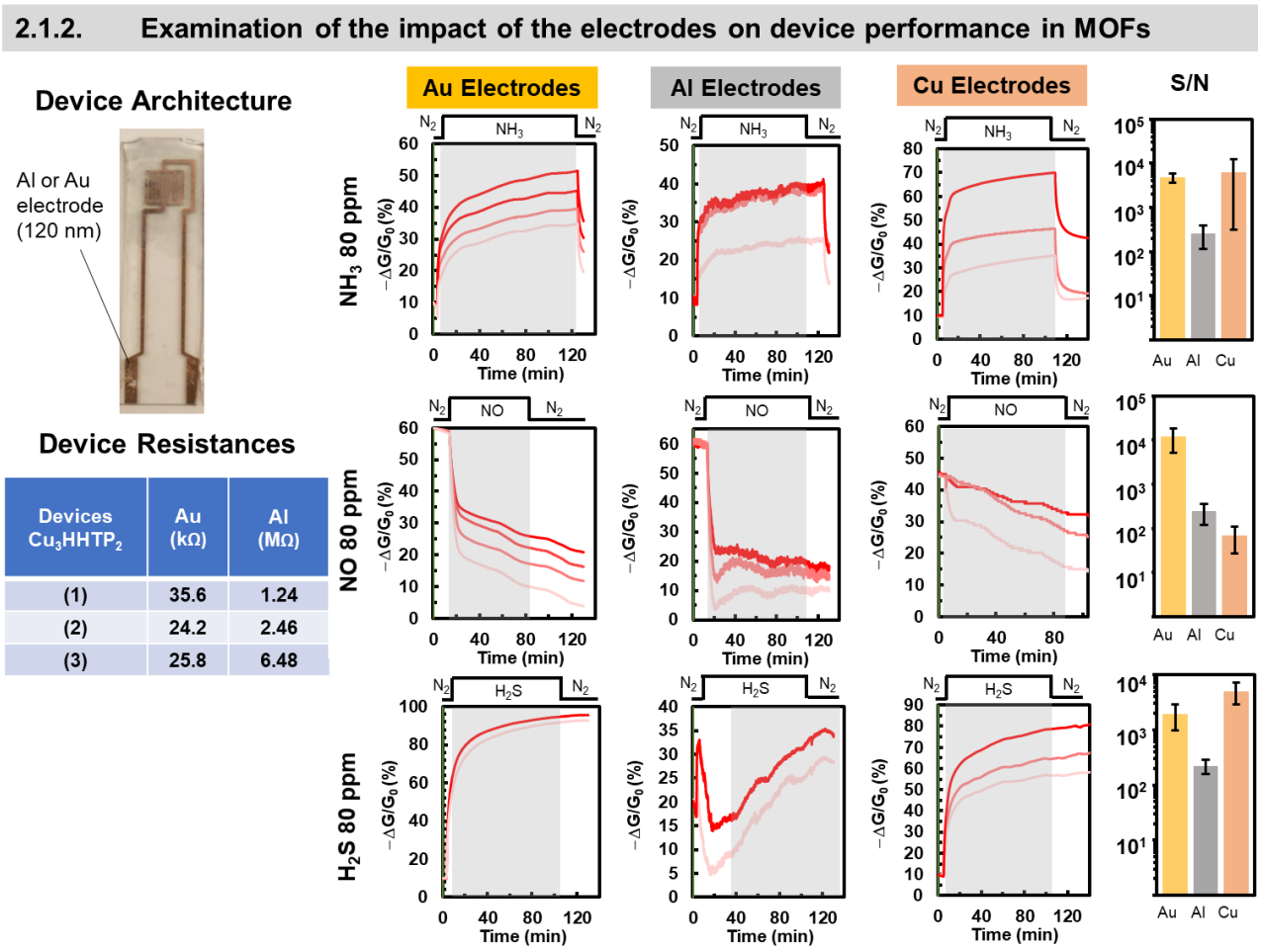

Figure 18. Progress towards Task 2.1.3. (a) Representation of configuration for the measurement of conductivity by four-point probe method and the voltage (*V*) and current (*A*) recorded. (b) The current change of a NiPc-Pyr pellet measured by a 2-point probe with as the temperature was increased from 293 to 393 K with an applied voltage of 1 V. (c) The Arrhenius plot of the current and temperature. (d) 2-point probe measurements of four M-COF-DC-8 as thin chemiresistive films. The applied voltage for for the thin film analysis was 1.0 V. (e) 4-point probe measurements performed on pressed pellets of M-COF-DC-8.

2.1.3. Electronic property study of MPc-based COFs

(a)

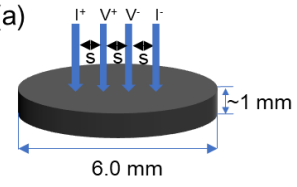

V (mV)	*I* (μA)
2.8	0.018
3.1	0.0205
35.7	0.153

(b)

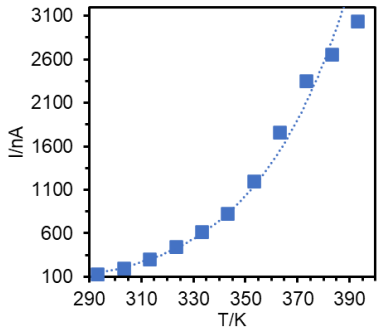

(c)

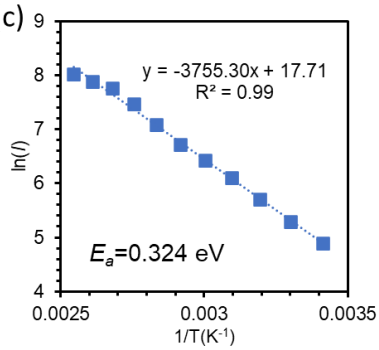

(d) 2-point probe thin film conductivity

M-COF-DC-8	σ (S/cm)	Error (S/cm)
Fe-COF-DC-8	6.3×10^{-5}	1.1×10^{-5}
Co-COF-DC-8	2.5×10^{-5}	5.9×10^{-6}
Ni-COF-DC-8	2.8×10^{-5}	7.52×10^{-6}
Cu-COF-DC-8	3.2×10^{-5}	5.5×10^{-6}

(e) 4-point probe pressed pellet conductivity

M-COF-DC-8	σ (S/cm)
Fe-COF-DC-8	1.1×10^{-4}
Co-COF-DC-8	3.8×10^{-5}
Ni-COF-DC-8	2.5×10^{-5}
Cu-COF-DC-8	no reading

Figure 19. Progress towards Task 2.2.1. Electron paramagnetic resonance spectroscopy (EPR) at 77 K was used to study the concentration and location of unpaired spins in HHTP-based MOFs. The pristine MOFs of Ni and Co show EPR-silent spectra indicating that any singularly occupied molecular orbitals (SOMO) are antiferromagnetically coupled. The large absorbance of Cu_3HHTP_2 at g>2 indicates that the SOMO primarily resides on the Cu metal center. The interaction of Co_3HHTP_2+Co_3HHTP and Ni_3HHTP_2+Ni_3HHTP MOFs with NO showed no perturbation to the EPR spectrum. However, the interaction of Cu_3HHTP_2 with NO showed an increase in the spin-density in the material. A similar trend was observed for all three MOFs with NH_3. The interaction of the bilayer MOFs with H_2S showed a dramatic increase in the spin-density in the MOFs. The spin-density of Cu_3HHTP_2 showed a significant decrease but the EPR spectrum also detected a small g =2.005 peak indicating a new radical species in the system.

2.2.1. EPR studies of analyte binding in MOFs

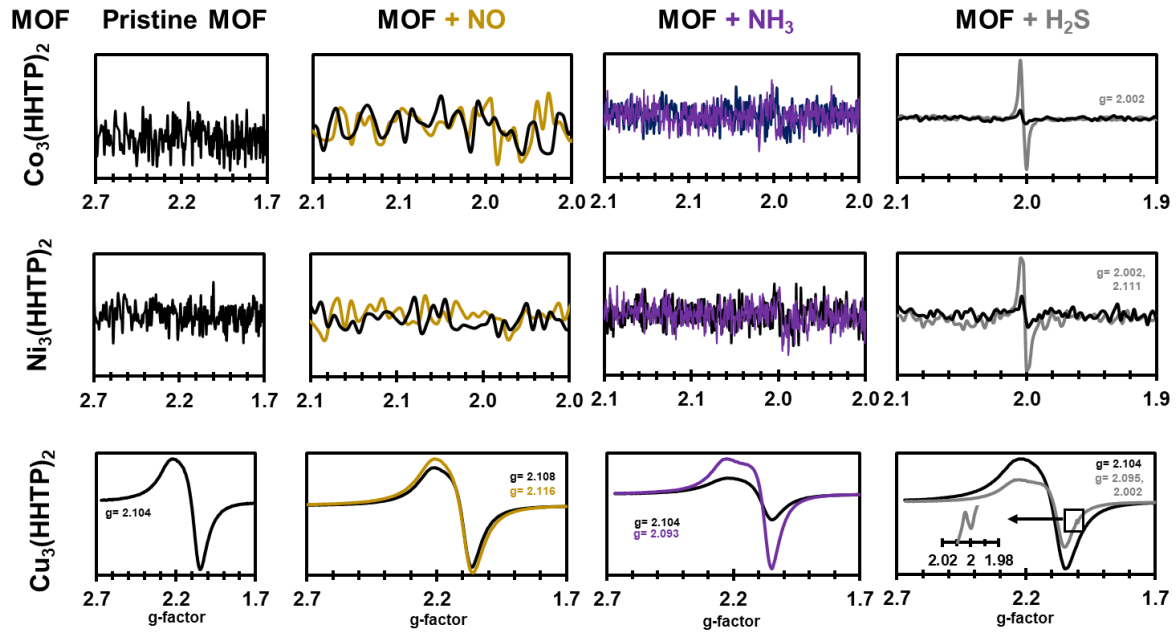

X-band EPR at 9.7 GHz, measurements taken at 77 K using 1-2 mg of sample

Samples degassed for 1 h with house N_2. The EPR spectrum was then taken (black trace). After initial analysis, the samples were exposed to a desired analyte gas at 1 % (balance N_2) for 20 min. Then a second spectrum was taken. MOFs were washed with water then with acetone in a Soxhlet extractor for 24-48 h. MOFs were dried under high vacuum and stored under argon unless otherwise noted.

Figure 20. Progress towards Task 2.2.1. Electron paramagnetic resonance spectroscopy (EPR) at 77 K was used to study the concentration and location of unpaired spins in HITP-based MOFs. The pristine MOFs of Ni show strong g=2.00 values. The large absorbance of Cu_3HITP_2 at g>2 indicates that the SOMO primarily resides on the Cu metal center. The interaction and Ni_3HHTP_2 with NO showed a small decrease in signal intensity suggesting that some radical residing on HITP ligand was quenched by the radical on NO. Cu_3HITP_2 showed an increase in signal intensity suggesting that NO caused a conversion of Cu^{I} to Cu^{II} upon exposure. An opposite trend was observed for Cu_3HITP_2 with NH_3, while Ni_3HITP_2 showed no response to NH_3. Ni_3HITP_2 responded similarly to H_2S showing no observable changes in radical spin density. Cu_3HITP_2 showed a shift int g-value as well as a new radical species in response to H_2S that was not metal-centered.

2.2.1. EPR studies of analyte binding in MOFs

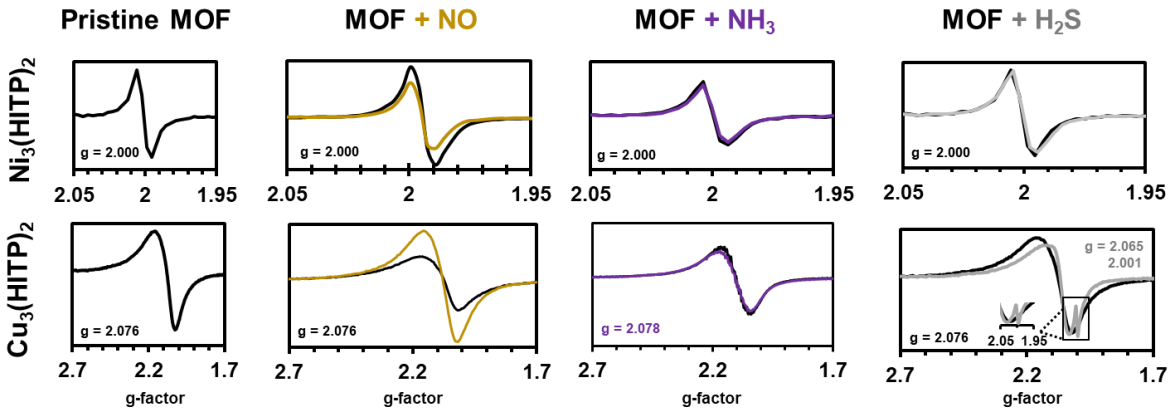

X-band EPR at 9.7 GHz, measurements taken at 77 K using 1-2 mg of sample

Samples degassed for 1 h with house N_2. The EPR spectrum was then taken (black trace). After initial analysis, the samples were exposed to a desired analyte gas at 1 % (balance N_2) for 20 min. Then a second spectrum was taken. MOFs were washed with water then with acetone in a Soxhlet extractor for 24-48 h. MOFs were dried under high vacuum and stored under argon unless otherwise noted.

Figure 21. Progress towards Task 2.2.1.
Electron paramagnetic resonance spectroscopy (EPR) at 77 K was used to study the concentration and location of unpaired spins in HHTP and HITP-based MOFs. For Ni_3HITP_2, oxygen caused a decrease in the intensity of the signal at g= 2.00. Ni_3HHTP_2 showed an increase in signal intensity at g= 2.00. Both Cu_3HITP_2 and Cu_3HHTP_2 showed a reduction in signal intensity in response to oxygen exposure. These results indicate that oxygen plays a significant role in the oxidation state of the MOF components and the charge balance within the framework.

2.2.1. EPR studies of analyte binding in MOFs

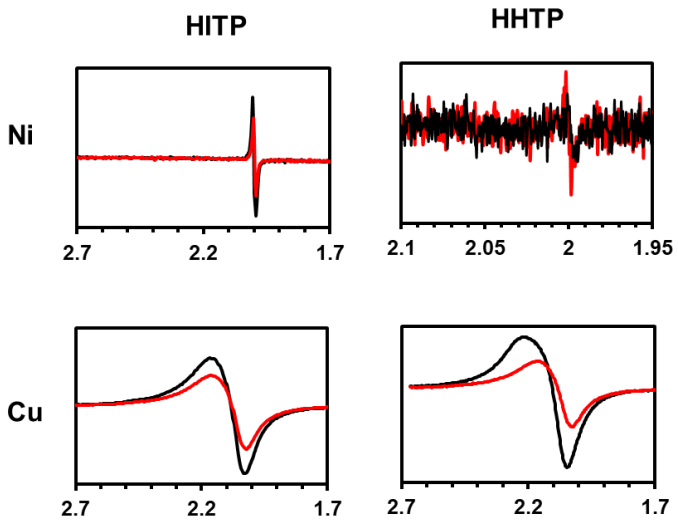

X-band EPR at 9.7 GHz, measurements taken at 77 K using 1-2 mg of sample

Samples degassed for 1 h with house N_2. The EPR spectrum was then taken (black trace). After initial analysis, the samples were exposed to a desired analyte gas at 1 % (balance N_2) for 20 min. Then a second spectrum was taken. MOFs were washed with water then with acetone in a Soxhlet extractor for 24-48 h. MOFs were dried under high vacuum and stored under argon unless otherwise noted.

Figure 22. Progress towards Task 2.2.1. XPS was used to determine the effects of NH_3 binding to MOF samples. The presence of a persistent N 1s emission line for HHTP-Based MOFs demonstrated that NH_3 binds irreversibly under the high-vacuum conditions of XPS. Further characterization of XPS was performed using high-resolution regions corresponding to specific analytes.

2.2.1. XPS studies of NH_3 confirms adsorption on MOF surface

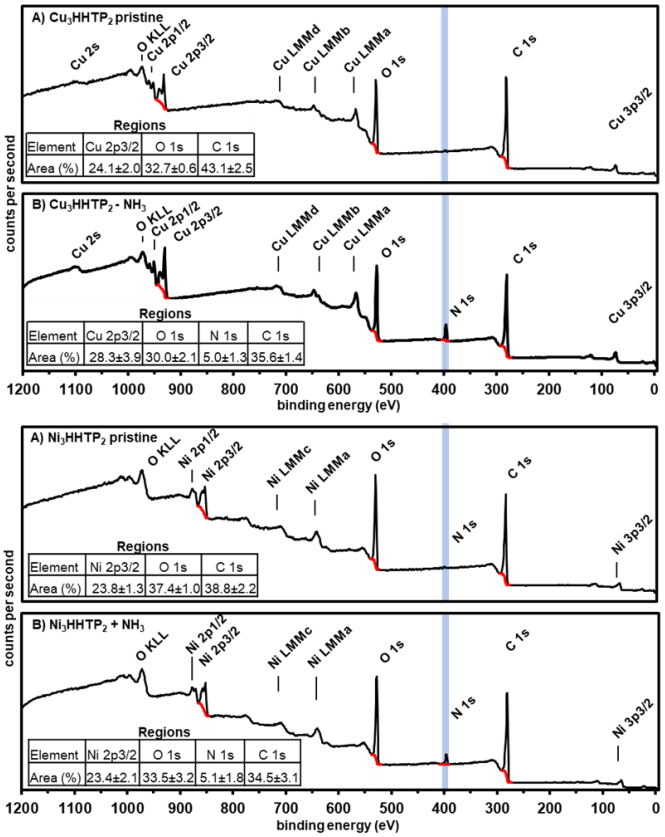

Figure 23. Progress towards Task 2.2.1.
Comparison of pristine and NH_3-exposed samples by XPS can reveal metal-oxidation state shifts by close examination of the metal 2p3/2 regions. **a)** pristine $Cu_3(HITP)_2$ shows a higher ratio of shakeup satellite emission line to primary Cu2p3/2 emission line when compared to NH_3 exposed $Cu_3(HITP)_2$. This indicates an increase in Cu^{II} and a concomitant decrease in Cu^{I}. **b)** pristine $Cu_3(HHTP)_2$shows a lower ratio of shakeup satellite emission line to primary Cu $2p_{3/2}$ emission line when compared to NH_3 exposed $Cu_3(HHTP)_2$. **c)** These shifts in intensity indicated a decrease in Cu^{II} and a concomitant increase in Cu^{I} for $Cu_3(HITP)_2$ and, for $Cu_3(HHTP)_2$, increase in Cu^{II} and a concomitant decrease in Cu^{I}.

2.2.1. XPS studies of NH_3 binding, and oxidation state changes of Cu in MOFs

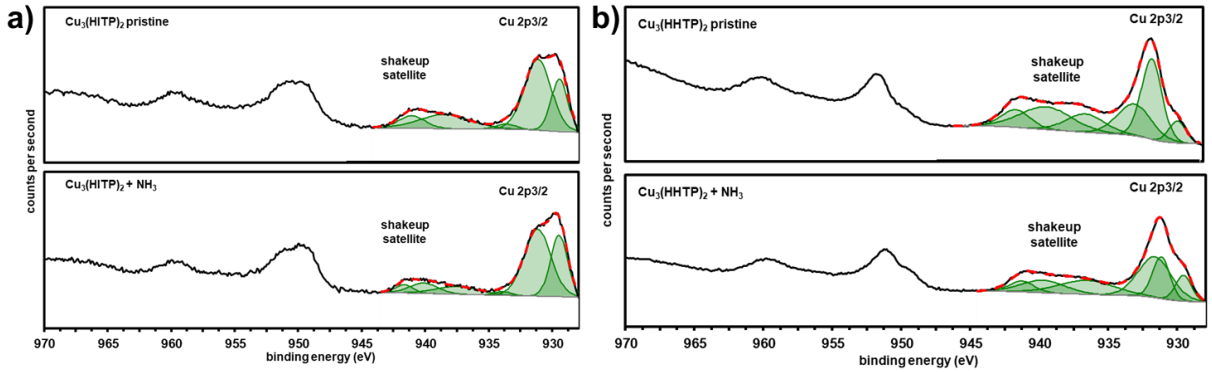

c)

MOF-analyte	% Cu^{II} by XPS	% Cu^{II} by EPR	Δ% Cu^{II} by XPS	Δ% Cu^{II} by EPR
$Cu_3(HITP)_2$	57.7±1	36.1±4	na	na
$Cu_3(HITP)_2$+NH_3	51.5±1	33.4±4	-6.2±1	-2.7±2
$Cu_3(HHTP)_2$	85.3±1	81.7±2	na	na
$Cu_3(HHTP)_2$+NH_3	95.3±3	93.5±2	+10.0±2	+12.9±3

Figure 24. Progress towards Task 2.2.2. EPR characterization of a) FePc-Pyr COF, b) CoPc-Pyr COF, c) NiPc-Pyr-COF, and d) CuPc-Pyr COF. Measurements were taken at 77 K after the material was flushed with N_2 for 24 h.

2.2.2. EPR spectroscopy of MPc-COFs (M= Fe, Co, Ni, Cu)

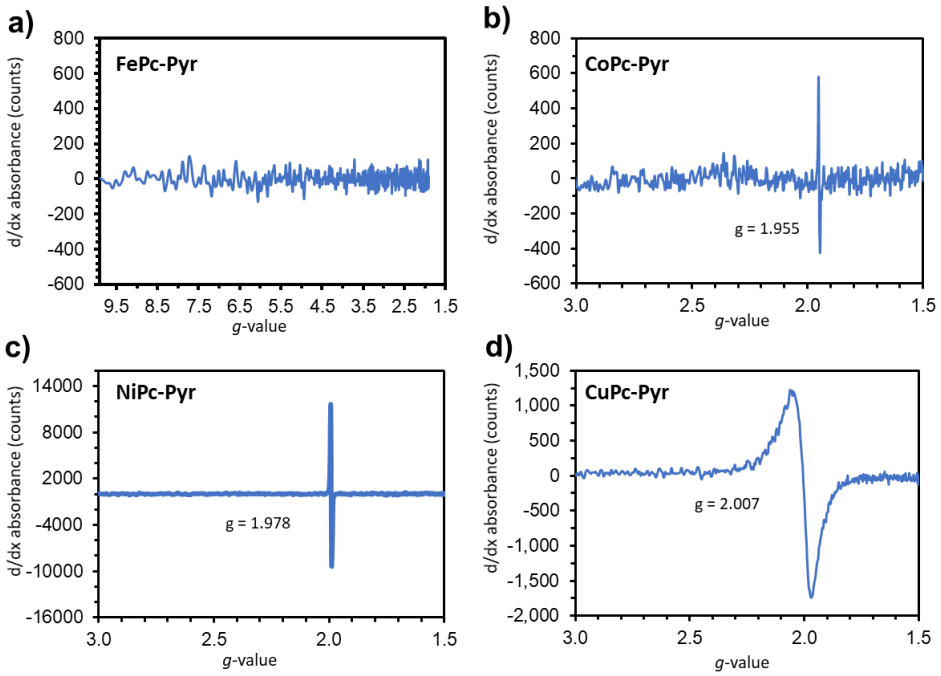

Figure 25. Progress towards Task 2.2.2. Comparison of the EPR spectra of (a) Fe-COF-DC-8, (b) Co-COF-DC-8, (c) Ni-COF-DC-8, and (d) Cu-COF-DC-8 before (black lines) and after (colored lines) dosing with (purple) NH_3, (green) NO, (gold) H_2S, and (grey) CO. EPR spectra were obtained at 4.2 K.

2.2.2. EPR studies of analyte binding in COFs

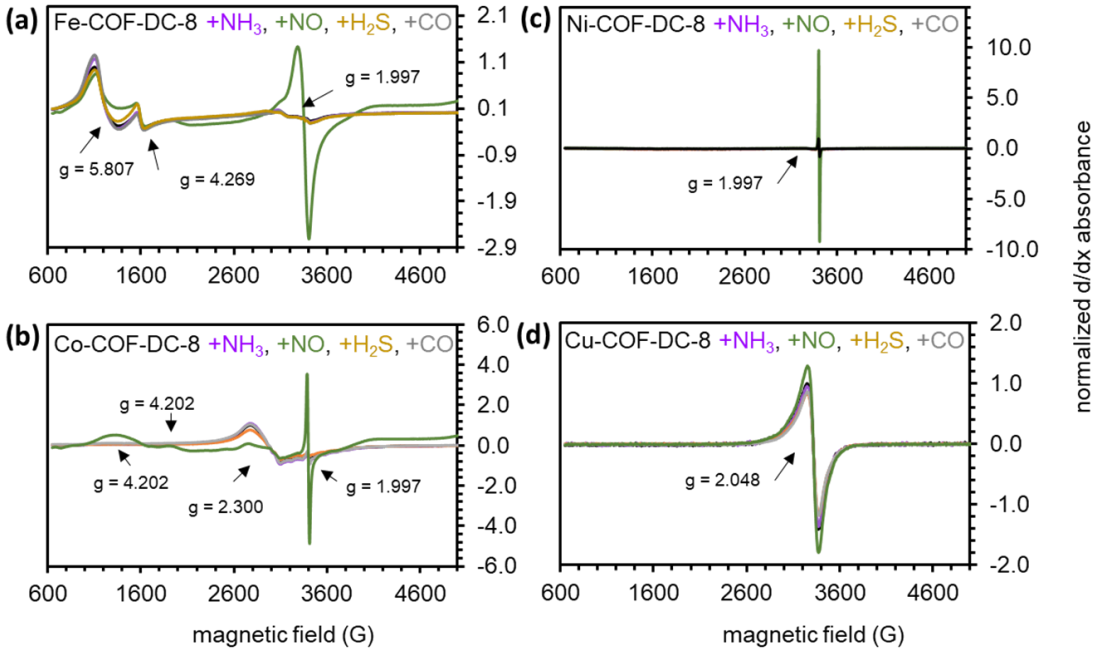

Figure 26. Progress towards Task 2.2.3. For each MOF, the temperature dependence of the molar magnetic susceptibility was measured from 300 K to 2 K.

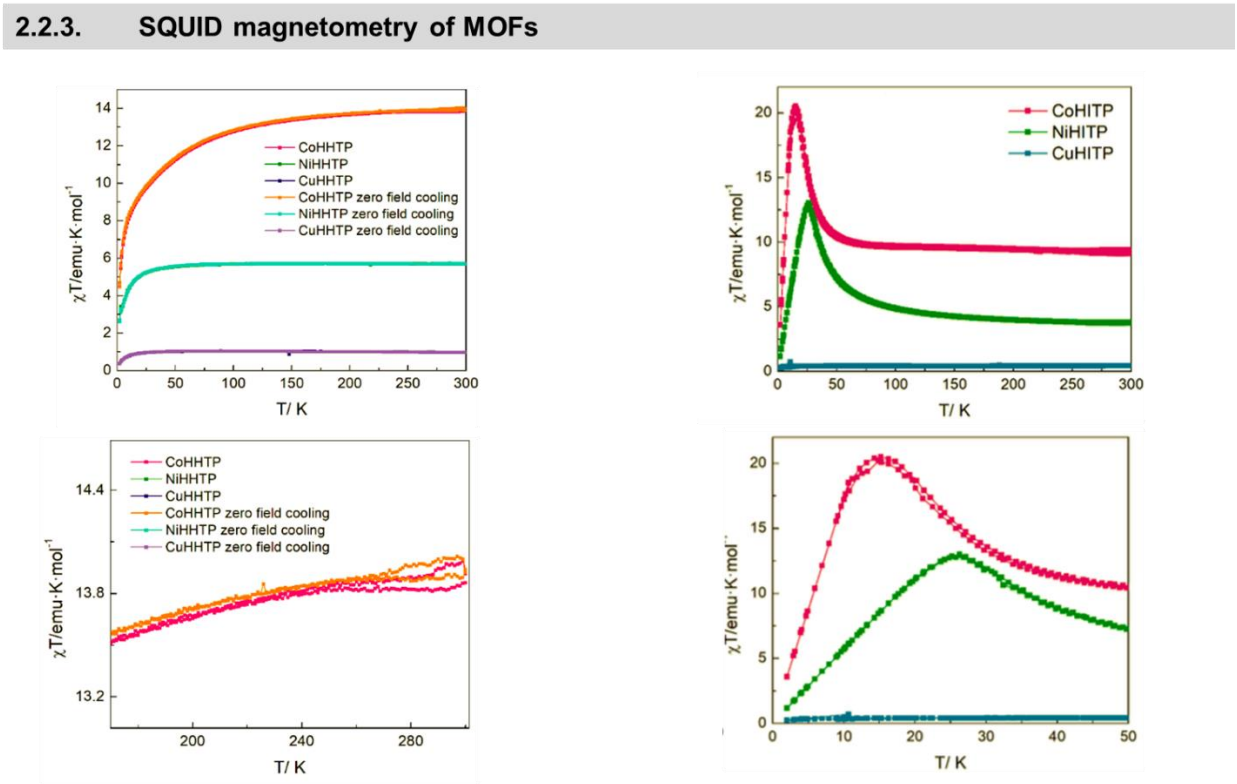

Figure 27. Progress towards Task 2.2.4. Computational modelling of spin-ordering in M-COF-DC-8 materials. (a) The band structure of Fe-COF-DC-8 in a high spin antiferromagnetically ordered spin state. (b) The band structure of Cu-COF-DC-8 in an antiferromagnetically ordered spin state. (c) the first Brillouin zone of COFs have I4-MMM symmetry enforced by spin orientation. (d) a graphical depiction of the antiferromagnetic ordering between metal centers in adjacent layers of the COFs.

2.2.4 Computational study of spin orientation and band structure

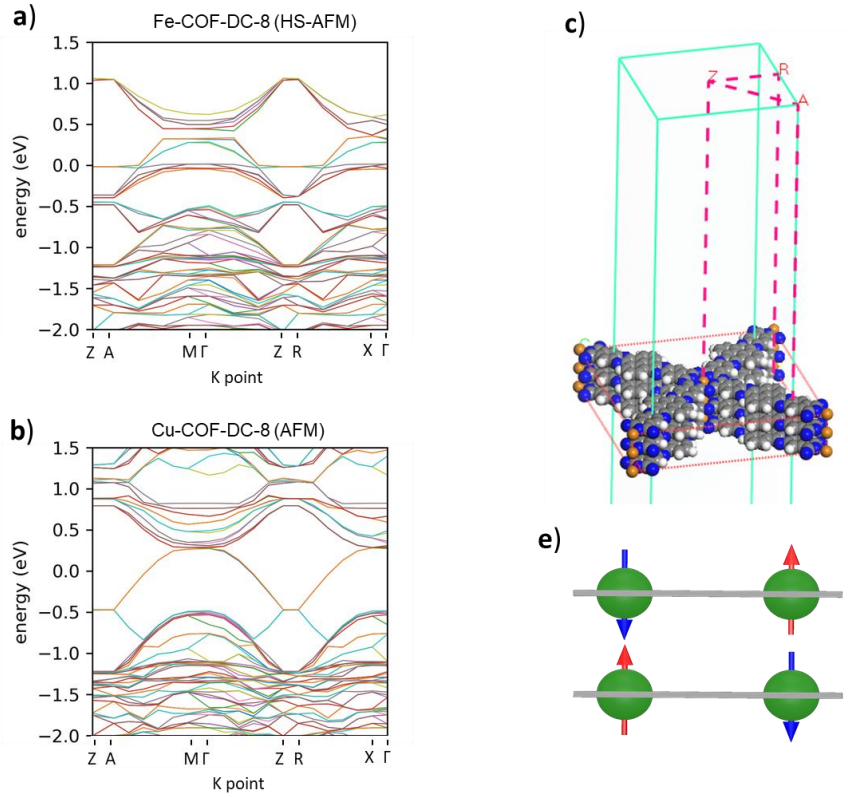

Table 1. Progress towards Task 3.1.1. MOFs are listed with their observed conductivities and their percent resistance changes normalized to their starting resistance in response to specified concentrations of gas. [a] 4-point probe method was used to obtain value. [b] 2-point probe method was used to obtain value

MOF	σ (S/cm)	NH_3 (–ΔG/G°) 80 ppm	H_2S (–ΔG/G°) 80 ppm	NO (–ΔG/G°) 80 ppb	CO (–ΔG/G°) 80 ppm
CoPc-Cu-NH	5.79×10^{-2} [a]	N/A	N/A	N/A	+ 30%
CoPc-Cu-O	2.12×10^{-2} [a]	N/A	N/A	N/A	+ 25%
NiPc-Cu-NH	2.73×10^{-3} [a]	N/A	N/A	N/A	+ 18%
NiPc-Cu-O	1.43×10^{-2} [a]	+ 45 %	+ 100 %	-120 %	+ 28%
NiPc-Ni-O	7.22×10^{-4} [a]	+ 43 %	+ 25 %	-80 %	N/A
$Cu_3(HHTN)_2$	9.01×10^{-8} [a]	N/A	N/A	N/A	N/A
$Ni_3(HHTP)_2$/cotton	1.6×10^{-4} [b]	- 80 %	+ 100 %	- 45 %	
$Ni_3(HITP)_2$/cotton	2.6×10^{-4} [b]	0 %	+ 98 %	+ 80 %	

Table 2. Progress towards Task 3.1.2. COFs are listed with their observed conductivities (obtained from thin films and 2-point probe at and applied voltage of 1.0 V) and their percent resistance changes normalized to their starting resistance in response to specified concentrations of gas.

COF	σ (S/cm)	NH_3 (–ΔG/G°) 80 ppm	H_2S (–ΔG/G°) 80 ppm	NO (–ΔG/G°) 80 ppb	CO (–ΔG/G°) 80 ppb
Fe-COF-DC-8	6.3×10-5	+ 29.1 %	+ 70.0 %	- 1644 %	+ 17.5 %
Co-COF-DC-8	2.5×10-5	+ 87.8 %	+ 72.8 %	- 5665 %	0 %
Ni-COF-DC-8	2.8×10-5	+ 35.2 %	+ 76.3 %	- 3049 %	0 %
Cu-COF-DC-8	3.2×10-5	+ 77.8 %	+ 99.3 %	- 7235 %	0 %

Figure 28. Progress towards Task 3.1.1 Magneto-transport studies using the 4-point probe devices was carried out using $Ni_3(HHTP)_2$. Resistance values were obtained over a range of B_0 field strengths ranging from 0 T to 0.8 T. Control studies were run using a B_0 strength of 0 T for the duration of the experiment. The relative increase in resistance values observed above B_0 > 0.6 T correlate with field strength when compared to control experiments.

3.1.1. Measurements of field effect in MOFs

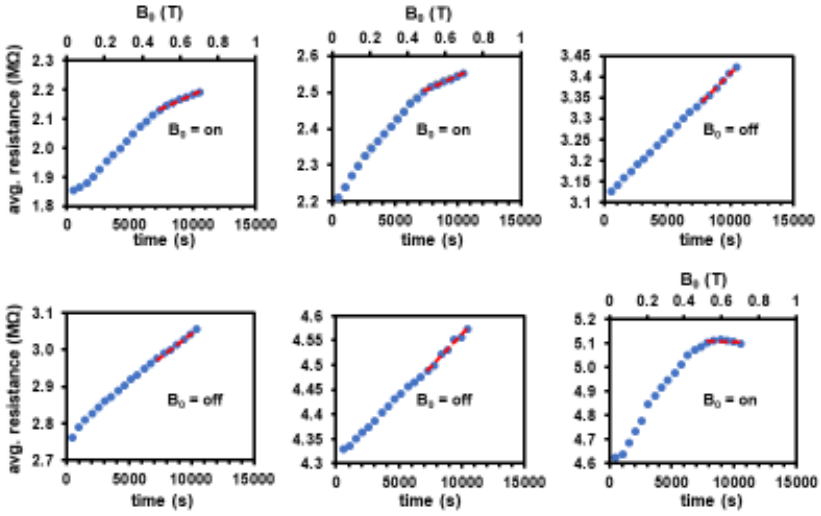

Device:
Ni_3HHTP_2 nanosheets deposited on gold electrode.

Experiment:
The B_0 field was scanned from 0 – 1 T with I/V curves taken at every 0.05 T increment. Average resistance obtained from the I/V curves potted versus B_0 (for B_0=on) or versus time (for B_0=off)
possible transition observed at B_0 = 0.6 T

Figure 29. Progress towards Task 3.2.1-3 Photographs of devices capable of interfacing small MOF sheets with 4-point probe measurements and magnetoelectronic instrumentation.

3.2.1. Fabrication of Hall Bar devices with MOFs
3.2.2. Measurements of charge mobility of MOFs
3.2.3. Measurements of field effect in MOFs

Magnetoresistance device and instrument setup

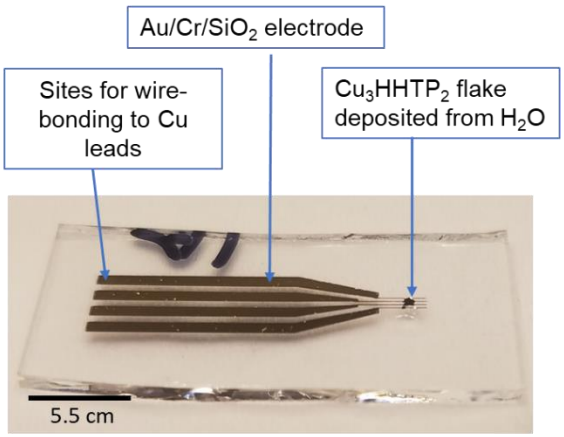

M_3HHTP_2 flake on Au-electrode device (M=Cu,Ni)

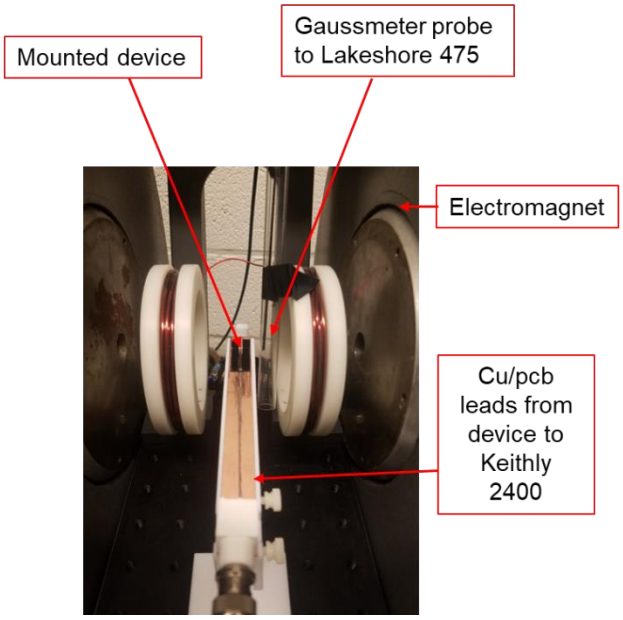

Figure 30. Progress towards Task 3.2.1. AFM analysis is a powerful method of characterizing thin freestanding films. The films used for magneto-transport studies were imaged by AFM (a) to determine (b) average thickness and average roughness.

3.2.1. Characterization of nanosheets by AFM

Magnetoresistance device and instrument setup

a)

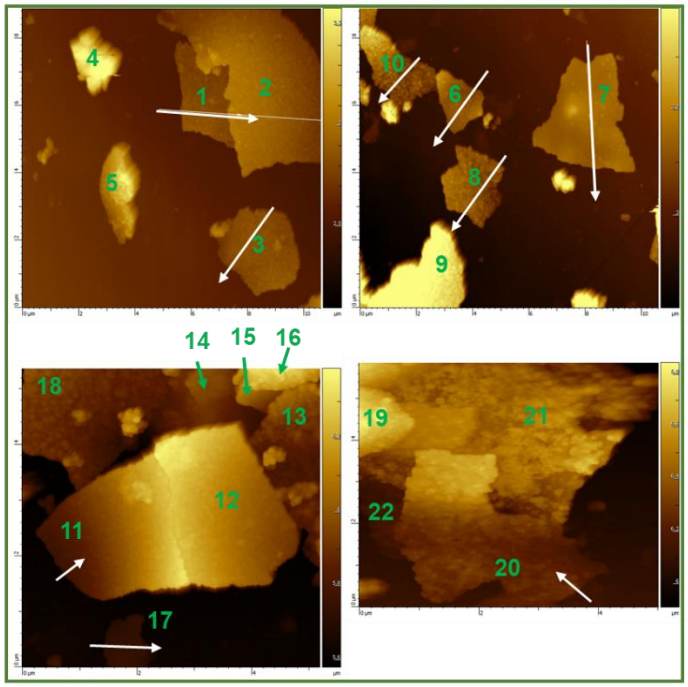

b)

NS number	Thickness (nm)	σ (nm)
1	288.2	18.1
2	204.3	22.9
3	301.9	50.9
6	170.1	13.4
7	159.5	28.2
8	187.7	34.5
10	156.3	25.8
11	163.9	5.8
17	116.3	5.9
20	93.3	8.0
Average thickness (nm)	184.1	-
σ (nm)	66.6	14.3

Figure 31. Progress towards Task 3.2.2 CPD analysis of (a) nanorods and (b) nanosheets under illumination demonstrate that the photovoltage changes as a function of morphology. Nanorods exhibit a positive photovoltage response (c), while nanosheets exhibit a negative photovoltage response (d).

3.2.1. Photovoltage response of different morphologies

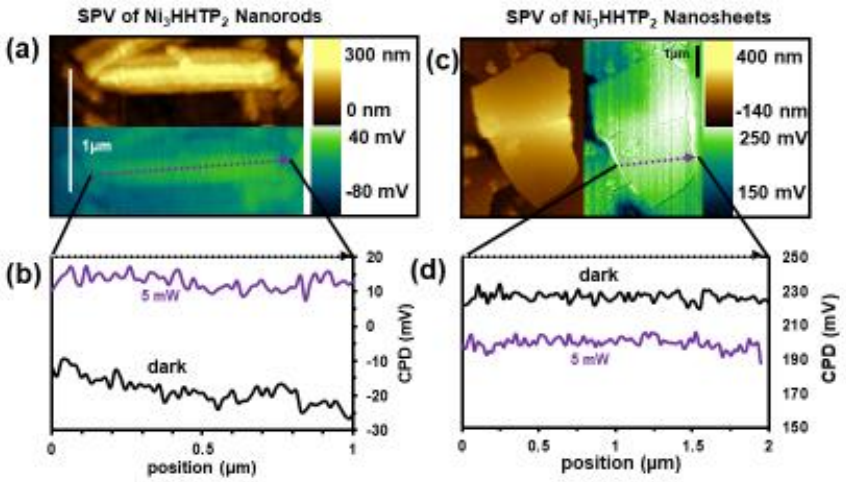

Figure 32. Progress Towards Task 3.2.4. Performance of chemiresistive device of NiPc-M MOFs. (a–c) Representative response of NiPc-Ni MOF to NH_3, H_2S, and NO at different concentrations. (d–f) Representative responses of NiPc-Cu MOF to NH_3, H_2S, and NO at different concentrations. (g–i) Responses (−ΔG/G0) of NiPc-Ni (green) and NiPc-Cu (blue) after 1.5 min exposure versus concentration of NH_3, H_2S, and NO. Suspensions of NiPc-M MOF were drop cast onto prefabricated electrodes and allowed to air dry to form chemiresistive devices. Prefabricated devices were composed of interdigitated gold electrodes on glass with 5 μm spacings between interdigitated electrode fingers

3.2.4 Charge mobility in NiPc-M MOF modulated by gas adsorption

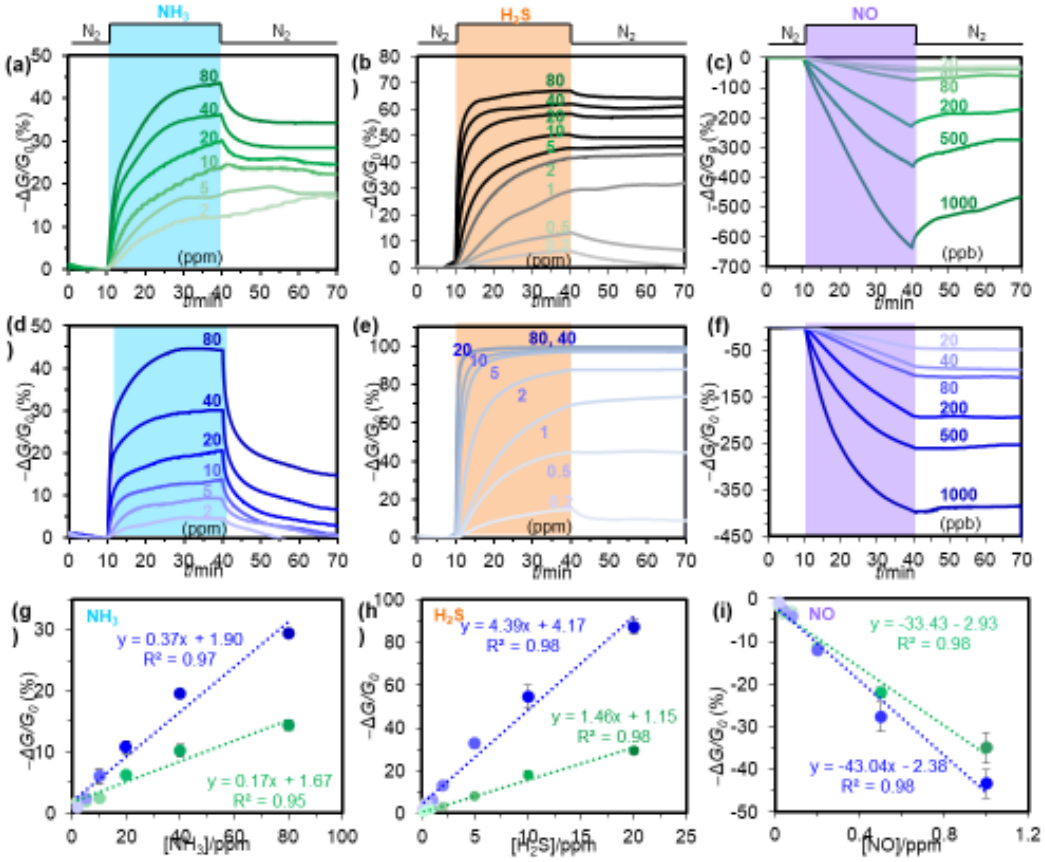

Figure 33. Progress Towards Task 3.2.4. Saturation sensing traces of (a) CoPc-O_8-Cu, (b) , (d) CoPc-$(NH)_8$-Cu, and (d) NiPc-$(NH)_8$-Cu MOF after 30 min exposure to 80, 40, 20, and 10 ppm of CO. (c) Responses ($-\Delta G/G_0$) of and CoPc-O_8-Cu MOF and NiPc-O_8-Cu after 30 min exposure versus concentration of CO. (c) (f) Responses of and CoPc-$(NH)_8$-Cu MOF and NiPc-$(NH)_8$-Cu after 30 min exposure versus concentration of CO. Sensing traces of (g) CoPc-O_8-Cu, (h) , (j) CoPc-$(NH)_8$-Cu, and (k) NiPc-$(NH)_8$-Cu MOF after 30 min exposure to 80 of CO in air. (i) Response of CoPc-O_8-Cu (blue) and NiPc-O_8-Cu (green) to 80 ppm CO in N_2, air, and 5000 ppm humidity. (l) Response of CoPc-$(NH)_8$-Cu (orange) and NiPc-$(NH)_8$-Cu (red) to 80 ppm CO in N_2, air, and 5000 ppm humidity.

3.2.4 Charge mobility in MPc-M MOF modulated by CO adsorption

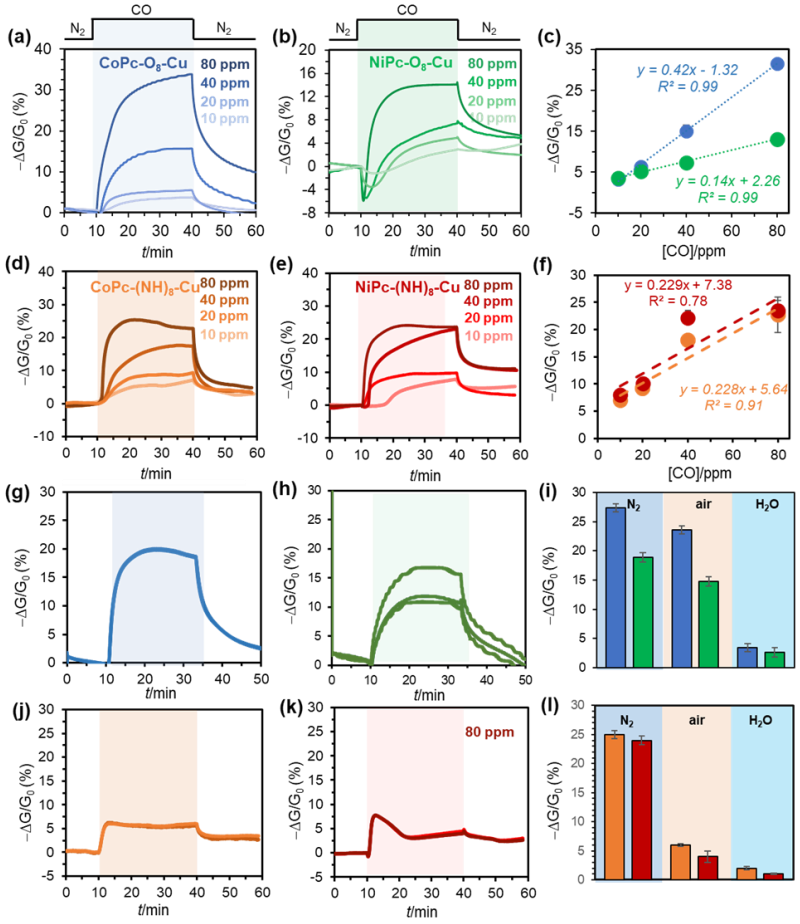

Figure 34. Progress Towards Tasks 3.2.6 and 3.2.7. Thin-film transistors (TFT) can probe materials for their charge transport properties, and performance under gated electric fields. NiPc-Pyr COF was drop cast onto TFT gates and the transistor performance was measured. a**)** optical image of a TFT device with NiPc-Pyr film covering the gate and connecting the Au source to drain. b**)** The on/off performance of a representative pristine TFT device showing a V_g on of -2 V. c**)** after NiPc-Pyr was drop cast on the device the V_g on shifted to +8 V.

3.2.6-7 Thin film transistors (TFT) containing COF films

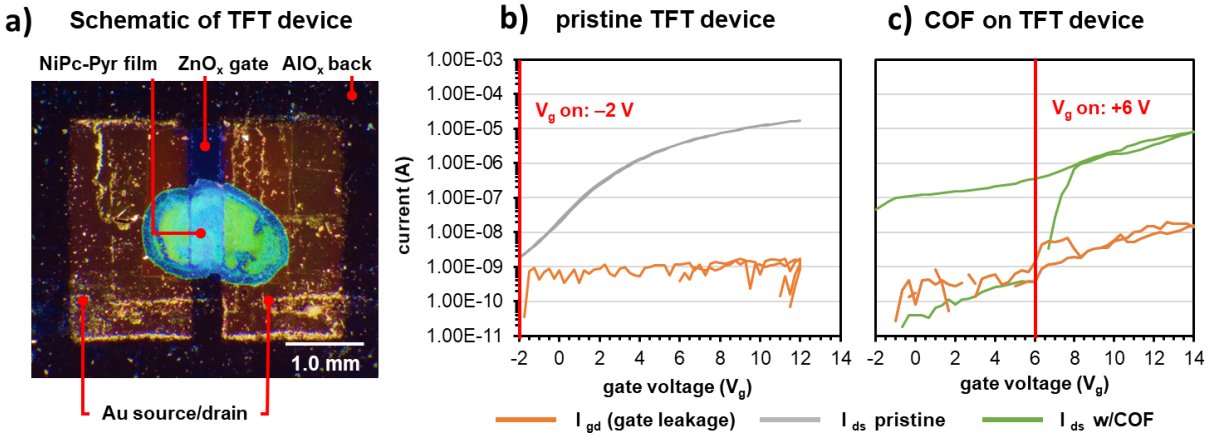

Figure 35. Progress Towards Task 3.2.8. Chemiresistive responses of devices with one of four unique MPc-Pyr COFs to (bottom row) NH_3, (2nd from bottom row) H_2S, (2nd from top row) CO, and (top row) NO under an applied voltage of 1.0 V and an atmosphere of dry nitrogen. Metal-dependent responses are observed for gas-MPc combinations. Suspensions of MPc-Pyr COF were drop cast onto prefabricated electrodes and allowed to air dry to form chemiresistive devices. Prefabricated devices were composed of interdigitated gold electrodes on glass with 5 μm spacings between interdigitated electrode fingers.

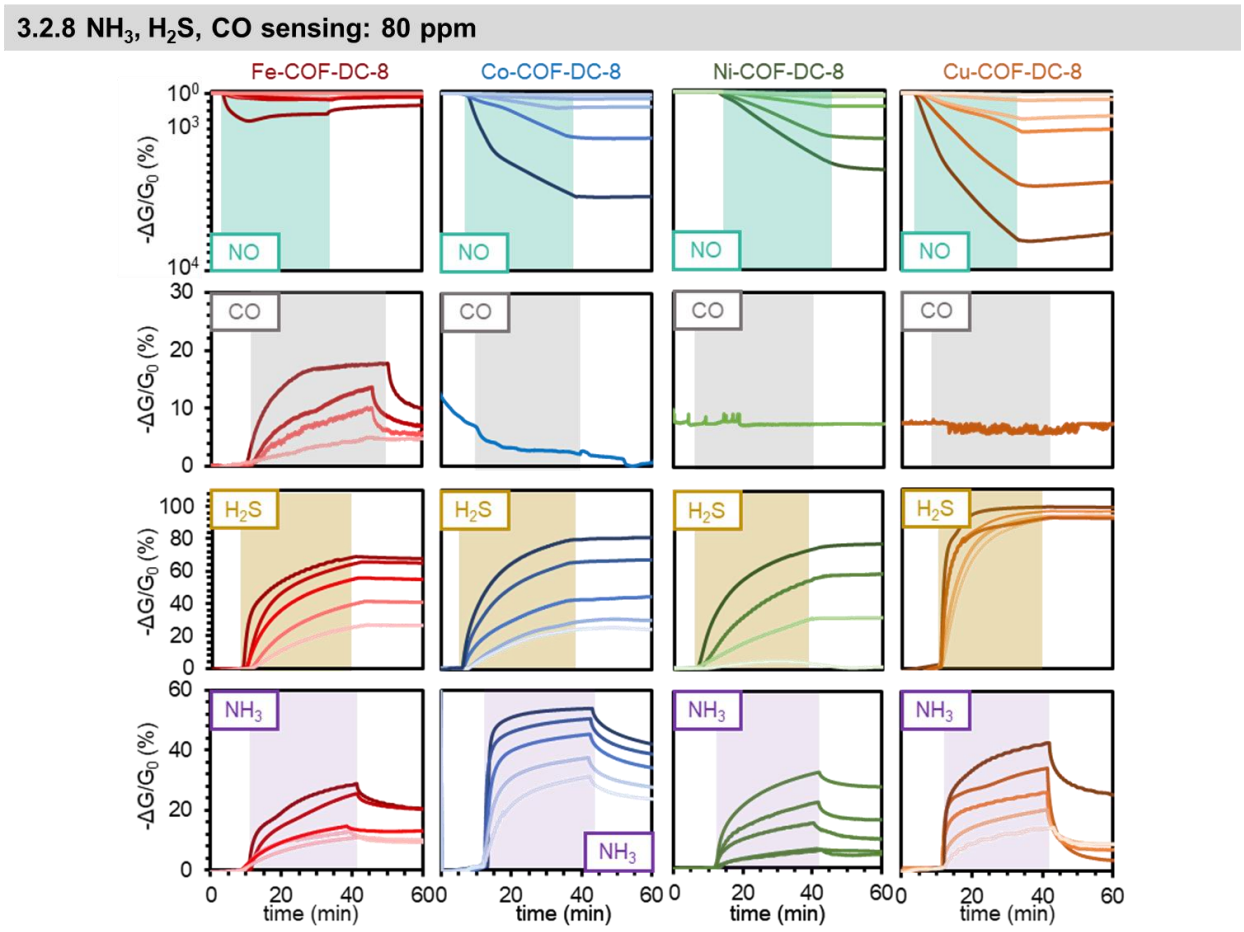

Figure 36. Progress Towards Task 3.2.8. Chemiresistive responses of devices with integrated NiPc-Pyr COF to (a) NH_3, (b) H_2S, and (c) NO_x, under an applied voltage of 1.0 V. The carrier gas was changed to determine the sensing performance under dry nitrogen, humid nitrogen, and ambient air. Responses ($-\Delta G/G_0$) of COF-DC-8. Suspensions of MPc-Pyr COF were drop cast onto prefabricated electrodes and allowed to air dry to form chemiresistive devices. Prefabricated devices were composed of interdigitated gold electrodes on glass with 5 μm spacings between interdigitated electrode fingers.

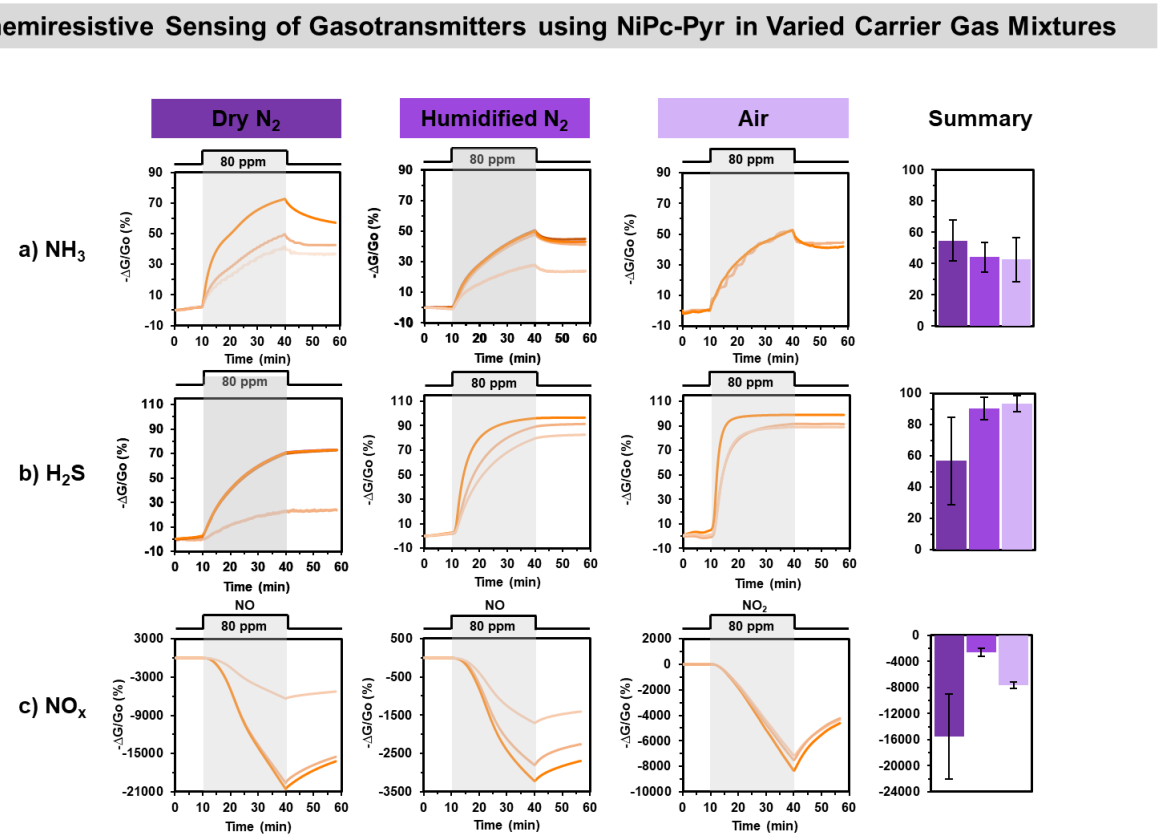

Figure 37. Progress Towards Task 3.2.8. Chemiresistive responses of devices with integrated NiPc-Pyr COF to (a) NH_3, (b) H_2S, and (c) NO, under an applied voltage of 1.0 V and an atmosphere of dry nitrogen. Responses ($-\Delta G/G_0$) of COF-DC-8 after 1.5 min (squares) and 30 min (circles) exposure versus concentration of (d) NH_3, (e) H_2S, and (f) NO. The LODs for these gases was NH_3: 70 ppb, H_2S: 204 ppb, and NO: 5 ppb. Suspensions of MPc-Pyr COF were drop cast onto prefabricated electrodes and allowed to air dry to form chemiresistive devices. Prefabricated devices were composed of interdigitated gold electrodes on glass with 5 μm spacings between interdigitated electrode fingers.

3.2.8 Charge mobility in NiPc-Pyr COF modulated by gas adsorption

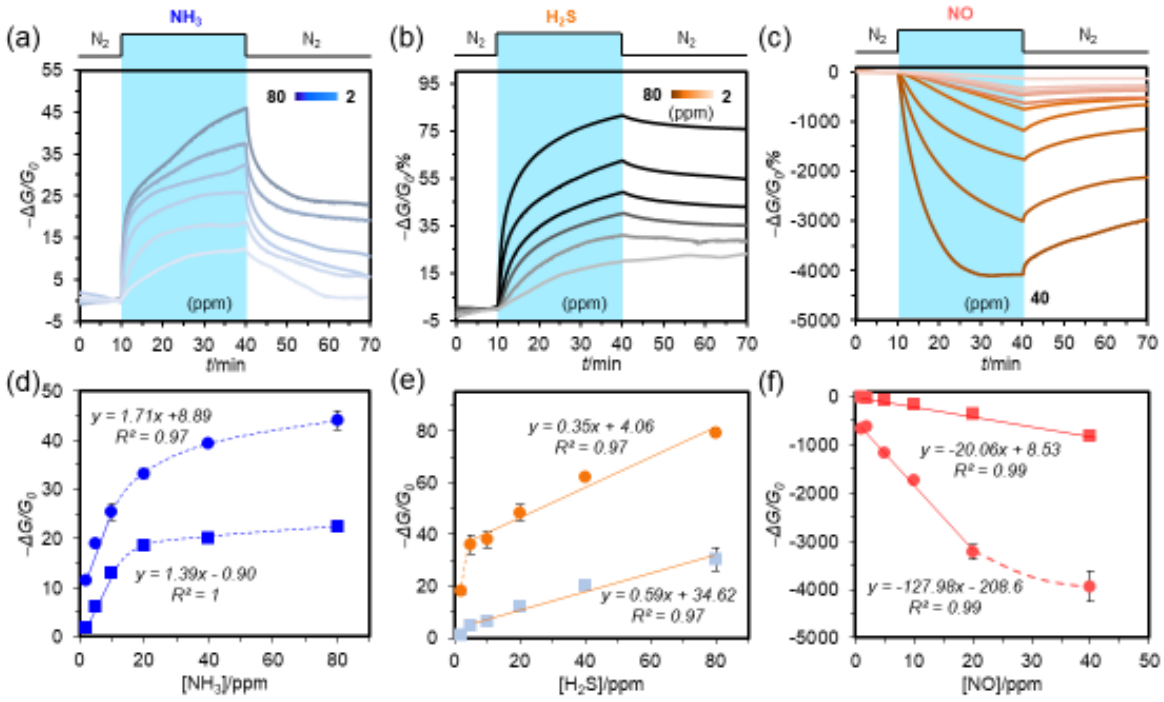

Figure 38. Contributions from HSAP/URAP. (a) Images of copper restructured into Cu_3HHTP_2 MOF demonstrated on a variety of substrates. (b) Oxidative restructuring enables enhanced stability of the MOF on these substrates even through chemical and physical stability tests by maintaining the signature MOF diffraction peaks. 2-point probe resistance measurements of MOF on cotton before and after each stability test.

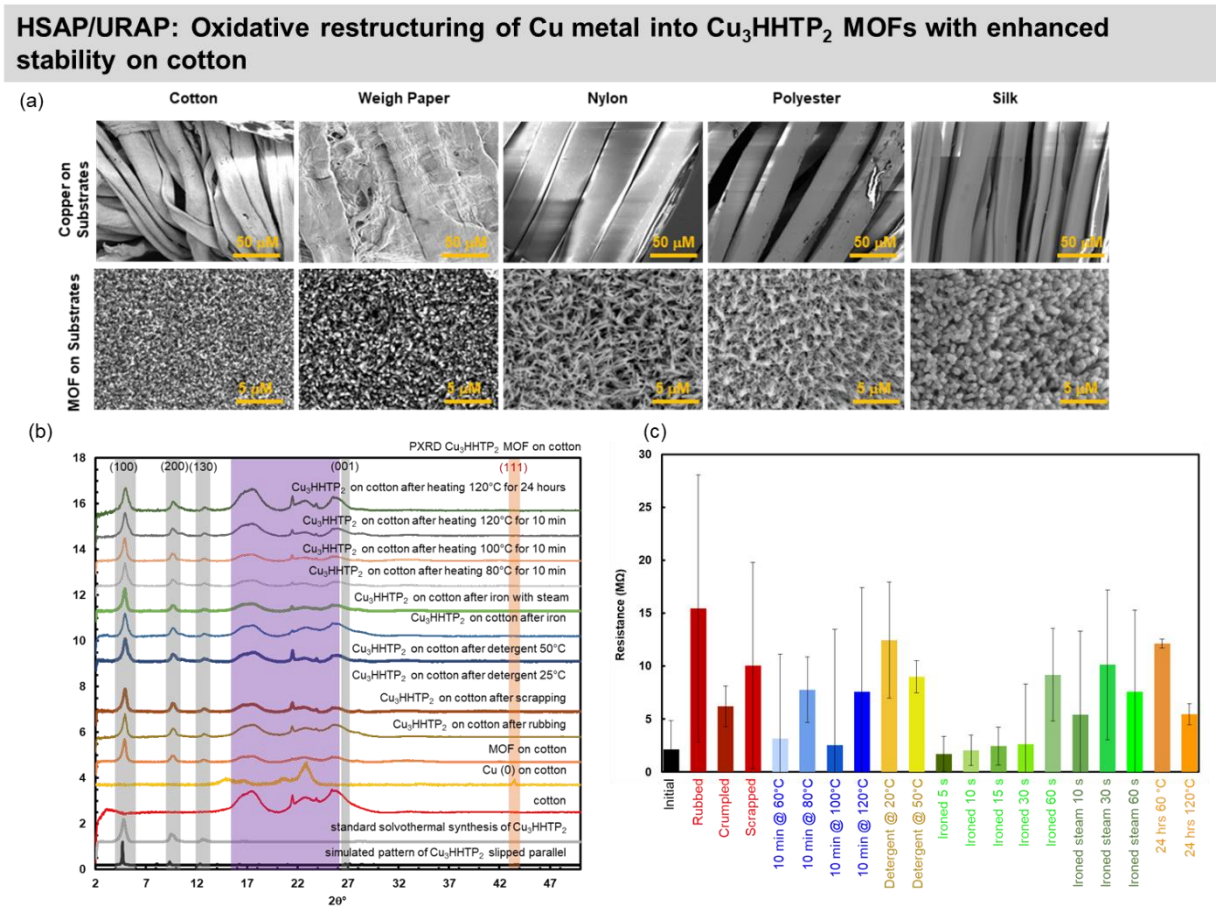

Figure 39. Contributions from HSAP/URAP. Chemiresistive sensing data using Cu_3HHTP_2 on cotton for the detection of H_2S at 80 ppm before and after the stability test. The response of the devices after the stability tests to H_2S after 100 minutes are comparable to the response of the newly fabricated devices.

HSAP/URAP: Chemiresistive sensing of H_2S with Cu_3HHTP_2 MOFs on cotton

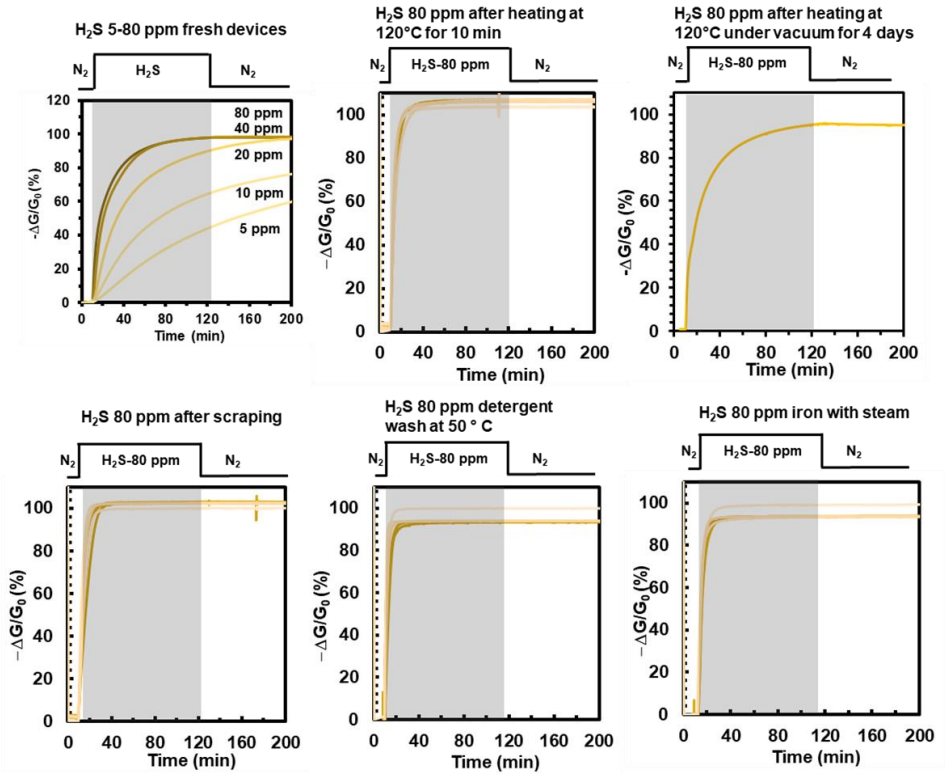

4) Key outcomes and other achievements.

- EPR assessment of analyte binding in MOFs and COFs shows perturbations of analytes to spin density of these materials.
- Synthetic access to novel COFs.
- Detection of gasotransmitters (NO, CO, H_2S) using a COF array
- The choice of materials as electrodes in devices plays a critical in determining device performance (e.g., signal-to-noise ratio, sensitivity).
- SQUID magnetometry of MOFs shows magnetic ordering of spins as a function of temperature.
- Both proposed MOFs and COFs exhibit substantial conductivity and chemiresistive response to gaseous analytes at part-per-million and part-per-billion concentrations.
- 13 papers published in peer reviewed journals acknowledging this grant since it has been awarded in 2017:

1. Ko, M.; Aykanat, A.; Smith, M. K.; **Mirica, K. A.*** "Drawing Sensors with Ball-Milled Blends of Metal-Organic Frameworks and Graphite" *Sensors* **2017**, *17*, 2192. Invited paper for a special issue "Chemiresistive Sensors: Status and the Future" co-edited with Prof. Timothy M. Swager.

2. Smith, M.; **Mirica, K. A.*** "Self-Organized Frameworks on Textiles (SOFT): Conductive Fabrics for Simultaneous Sensing, Capture, and Filtration of Gases" *J. Am. Chem. Soc.* **2017**, *139*, 16759–16767.

3. Mendecki, L; **Mirica, K. A.*** "Conductive Metal–Organic Frameworks as Ion-to-Electron Transducers in Potentiometric Sensors" *ACS Appl. Mater. Interfaces* **2018**, *10*, 19248–19257.

4. Ko, M.; Mendecki, L.; **Mirica, K. A.*** "Conductive two-dimensional metal–organic frameworks as multifunctional materials" *Chem. Commun*. **2018**, *54*, 7873-7891.

5. Meng, Z.; Stolz, R. M.; Mendecki, L.; **Mirica, K. A.*** "Electrically-Transduced Chemical Sensors Based on Two-Dimensional Nanomaterials" *Chem. Rev.* **2019**, *119*, 478–598.

6. Meng, Z.; Aykanat, A.; **Mirica, K. A.*** "Proton Conduction in 2D Aza-Fused Covalent Organic Frameworks" *Chem. Mater*. **2019**, *31*, 819–825.

7. Meng, Z.; Aykanat, A.; **Mirica, K. A.*** "Welding Metallophthalocyanines into Bimetallic Molecular Meshes for Ultrasensitive, Low-Power Chemiresistive Detection of Gases" *J. Am. Chem. Soc.* **2019**, *141*, 2046–2053.

8. Meng, Z.; Stolz, R.; **Mirica, K. A.*** "Two-Dimensional Chemiresistive Covalent Organic Framework with High Intrinsic Conductivity" *J. Am. Chem. Soc*. **2019**, *141*, 11929–11937.

9. Aykanat, A.; Meng, Z.; Bendetto, G.; **Mirica K. A.*** "Molecular Engineering of Multifunctional Metallophtalocyanine-Containing Framework Materials" *Chem. Mater*. **2020**, *32*, 5372–5409.

10. Ko, M.; Mendecki, L.; Eagleton, A.; Durbin, C. G.; Stolz, R. M.; Meng. Z.; **Mirica, K. A.*** "Employing Conductive Metal–Organic Frameworks for Voltammetric Detection of Neurochemicals" *J. Am. Chem. Soc.* **2020**, 142, 11717–11733

11. Stolz, R. M.; Mahdavi-Shakib, A.; Frederick, B. G.*; **Mirica, K. A.*** "Host–Guest Interactions and Redox Activity in Layered Conductive Metal–Organic Frameworks" *Chem. Mater*. **2020**, *32*, 7639–7652.

12. Meng, Z.; Luo, J.; Li, W.*; **Mirica, K. A.*** "Hierarchical Tuning of the Performance of Electrochemical Carbon Dioxide Reduction Using Conductive Two-Dimensional Metallophthalocyanine Based Metal−Organic Frameworks" *J. Am. Chem. Soc.* **2020**, *142*, 21656–21669.

13. Meng, Z.; **Mirica, K. A.*** "Two-Dimensional d-π Conjugated Metal−Organic Framework Based on Hexahydroxytrinaphthylene" *Nano Research* **2021**, *14*, 369–375.

- 6 patent applications have been filed acknowledging this grant:

1. "Self-Assembly of Metal-Organic Frameworks on Textiles" **Mirica, K. A.**; Smith, M. K.; U.S. Provisional Patent Application No. 62/489,851 filed on 04/25/2017. U.S. Utility Patent Application No. 15/962,156 filed on 04/25/2018.
2. "Metal-Organic Frameworks as Ion-to-Electron Transducers and Detectors" **Mirica, K. A.**; Mendecki, L; U.S. Provisional Patent Application No. 62/544,355 filed on 08/11/2017. PCT Patent Application No. 18/46,510 filed on 08/11/2018.
3. "Formation of Metal-Organic Frameworks" **Mirica, K. A.;** Ko, M.; Mendecki, L. U.S. Provisional Patent Application No. 62/681,436 filed on 06/06/2018. PCT Patent Application No. 19/35,727 filed on 06/06/2019.
4. "Conductive Metal-Organic Frameworks for Electrochemical Detection of Analytes" **Mirica, K. A.**; Mendecki, L.; Ko, M.; Meng, Z.; Stolz, R. M.; Eagleton, A. U.S. Provisional Patent Application No. 62/688,261 filed on 06/21/2018. PCT Patent Application No. 19/38,492 filed on 06/21/2019.
5. "Conductive Bimetallic Metal-Organic Frameworks for the Detection of Analytes" **Mirica, K. A.**; Meng, Z.; Aykanat, A. U.S. Provisional Patent Application No. 62/719,264 filed on 08/17/2018. PCT Patent Application No. 19/47,010 filed on 08/19/2019.
6. "Two-dimensional Stimuli-Response Covalent Organic Frameworks with High Intrinsic Conductivity" **Mirica, K. A.**; Meng, Z.; Stolz, R. M.; U.S. Provisional Patent Application No. 62/837,118 filed on 04/22/2019.